THESIS

PHYSIOCHEMICAL PROPERTIES AND EVAPORATION DYNAMICS OF BIOALCOHOL-GASOLINE BLENDS

Submitted by

Bahareh Abdollahipoor

Department of Mechanical Engineering

In partial fulfillment of the requirements

For the Degree of Master of Science

Colorado State University

Fort Collins, Colorado

Summer 2018

Master's Committee:

Advisor: Bret C. Windom

Kenneth F. Reardon
Daniel B. Olsen

ABSTRACT

PHYSIOCHEMICAL PROPERTIES AND EVAPORATION DYNAMICS OF BIOALCOHOL-GASOLINE BLENDS

After fermentation, the concentration of bioethanol is only 8-12 wt%. To produce anhydrous ethanol fuel, a significant amount of energy is required for separation and dehydration. Once the azeotrope composition is reached, distillation can no longer be exploited for purification and other expensive methods must be used. Replacing anhydrous ethanol fuel with hydrous ethanol (at the azeotrope composition) can result in significant energy and cost savings during production. Currently there is a lack of available thermophysical property data for hydrous ethanol gasoline fuel blends. This data is important to understand the effect of water on critical fuel properties and to evaluate the potential of using hydrous ethanol fuels in conventional and optimized spark ignition engines. In this study, the thermophysical properties, volatility behavior, evaporation dynamic, and mixing/sooting potential of various hydrous and anhydrous ethanol blends with gasoline were characterized. Results show that the properties of low and mid-level hydrous ethanol blends are not significantly different from those of anhydrous ethanol blends, suggesting that hydrous ethanol blends have the potential to be used in current internal combustion engines as a drop-in biofuel.

Dual-alcohol approach, mixing lower and higher alcohols with gasoline to obtain a blend with a vapor pressure close to that of the base gasoline, is a potential way to circumvent issues with single alcohol blends. In second project, the azeotropic volatility behavior and mixing/sooting

potential of dual-alcohol gasoline blends were studied by monitoring the distillation composition evolution and use of droplet evaporation model.

ACKNOWLEDGMENTS

I extend my gratitude to my academic advisor Dr. Bret Windom for his inspiration, continuous support, and timely guidance throughout my studies at Colorado State University. I am fortunate to be a part of his research team which helped me to grow not only in academics but as a complete individual. I owe my deepest gratefulness for his generous financial support for my studies.

I am thankful to my exam committee Dr. Daniel Olsen and Dr. Kenneth Reardon for their guidance, suggestions and contributions in editing this report.

I would like to thank all my group members but my special thank goes to Stephen Burke who helped me with the modeling part of my projects.

I especially would like to thank my dearest husband, Saeid Shirazi, for all his time and supports in all the life's challenges and during my graduate studies. I am so lucky to have the miracle of his presence in my life.

I would like to convey my deep gratitude to my beloved parents and brother whose emotional inspirations have been always been a motivation for me to chase my dreams. With no shadow of doubt, it is only their sacrifices that let me to be my perfect one who is always fighting for her goals.

DEDICATION

To my grandmother, *Masoumeh Shirazian*

The strong woman who always understood.

The faithful woman who always prayed for my success.

TABLE OF CONTENTS

ABSTRACT ii

ACKNOWLEDGMENTS iv

DEDICATION v

1 Introduction 1

1.2 Part I: Hydrous ethanol-gasoline mixtures 1

1.3 Part I: Research objective 3

1.4 Part II: Dual-alcohol blending approach 4

1.5 Part II: Research objective 5

2 Literature Review 6

2.1 Background 6

2.2 Biofuels 6

2.3 Bio-derived anti-pollution and octane enhancer additives 8

2.4 Alcohols as alternative biofuels 10

2.5 Spark-ignition engine 11

2.5.1 General effects of alcohols on SI engine performance 12

2.5.2 General effects of hydrous ethanol on SI engine performance 14

3 Experimental and numerical methods 18

3.1 Introduction 18

3.2 Test fuels 18

3.3 Experimental methods 18

3.3.1 Characterization tests 18

3.3.2 Volatility measurements and composition analysis 19

3.4 Distillation and droplet models 24

4 Azeotropic Volatility Behavior and Physiochemical Property Characterization of Hydrous and Anhydrous Ethanol Gasoline Mixtures 29

4.1 Background 29

4.2 Test fuels 30

4.3 Results and discussion 30

4.3.1 Volatility 31

4.3.2 Corrosion and water phase stability 51

4.3.3 Lower heating value 53

4.3.4 Viscosity and density 54

4.4 Conclusion 55

5 Volatility Behavior of Dual-alcohol Blends 57

5.1 Background 57

5.2 Test fuels 58

5.3 Results and discussion 59

5.4 Conclusion 73

6 Conclusions and Recommendations 74

6.1 Part I: Hydrous ethanol-gasoline mixtures 74

6.2 Part II: Dual-alcohol blending approach 76

7 References 78

1 Introduction

1.1 Background

Availability, cost constraints and global warming are main concerns with regard to fossil fuels. In recent years, biofuels have been considered as alternatives to fossil fuels because they can be derived from non-toxic, biodegradable, and potentially renewable resources while exhibiting less harmful environmental features [1]. In the United States, the Renewable Fuel Standard (RFS) created by the U.S. Environmental Protection Agency (EPA) calls for the production of 36 billion gallons of biofuels annually by 2022 to reduce greenhouse gas emissions and improve energy security [2]. Among biofuels, bio-ethanol in particular is expected to play a significant role in substituting fossil fuels. Bio-ethanol is produced from renewable sources and is relatively low cost. Despite having lower specific energy content than the gasoline it is replacing, ethanol possesses unique properties stemming from its molecular structure and oxygen content that can lend itself to improved combustion efficiency and a reduction in harmful exhaust emissions. Based on the most recent report from U.S. Energy Information Administration (EIA), fuel ethanol production capacity reached 15.5 billion gallons per year at the beginning of 2017 in the United States [3]. Almost all gasoline engine vehicles made after 2001 can use gasoline blends with 10 and 15 vol. % ethanol, E10 and E15 respectively. Flexible fuel vehicles (FFVs) can operate with significantly higher concentrations such as E85 and E100.

1.2 Part I: Hydrous ethanol-gasoline mixtures

In the United States, the ethanol blended in gasoline is anhydrous; i.e., a maximum water content of 1 wt% in ethanol based on the standard specification for fuel ethanol for automotive spark-ignition engines (ASTM D 5798-99). However, the ethanol produced from fermentation has a concentration of only 8-12 wt%; the rest is composed primarily of water along with organic

acids, carbon dioxide, and other trace species [4]. Thus, to produce the anhydrous ethanol fuel, a significant amount of energy is required for separation and dehydration. Shapouri et al. [5] conducted a study to identify the net energy value of corn ethanol. In their study, the total output energy based on the higher heating value of ethanol and co-products energy credits was estimated to be around 25 MJ/L. Based on this report, as shown in Figure 1.1., the energy required for water removal to obtain anhydrous ethanol accounts for 37% (~ 9.5 MJ/L) of the total output energy, including distillation (23% of total energy output) and dehydration (14% of total energy output) processes. Separating water and ethanol by way of distillation is a highly energy intensive process, especially when distillation-based separation techniques are applied to mixtures containing more than 90% ethanol. This is a result of azeotrope interactions; at the ethanol-water azeotrope point (95.6/4.4 wt% ethanol/water) no further separation can be achieved at constant pressure. Instead, additional energy must be provided to overcome this limitation [6, 7]. Once an azeotropic mixture forms, distillation can no longer be exploited for further purification [8]. Instead, methods such as membrane-distillation hybrids, pressure-swing distillation, entrainer-addition distillation methods, and molecular sieve separation techniques are required [9,10]. These alternate methods add expense, complexity, and energy requirements. The expense of anhydrous ethanol production suggests opportunities for improvements from economic, energy, and greenhouse gas points of view. One option to address these shortcomings is to use hydrous ethanol (at the water/ethanol azeotropic mass fraction) blended with gasoline as a fuel in internal combustion engines. This could save up to 14% of the fuel energy during its production (~3.5 MJ/L) [5]. However, questions related to the water addition and its impact on engine operation, fuel economy, and fuel supply systems must be answered.

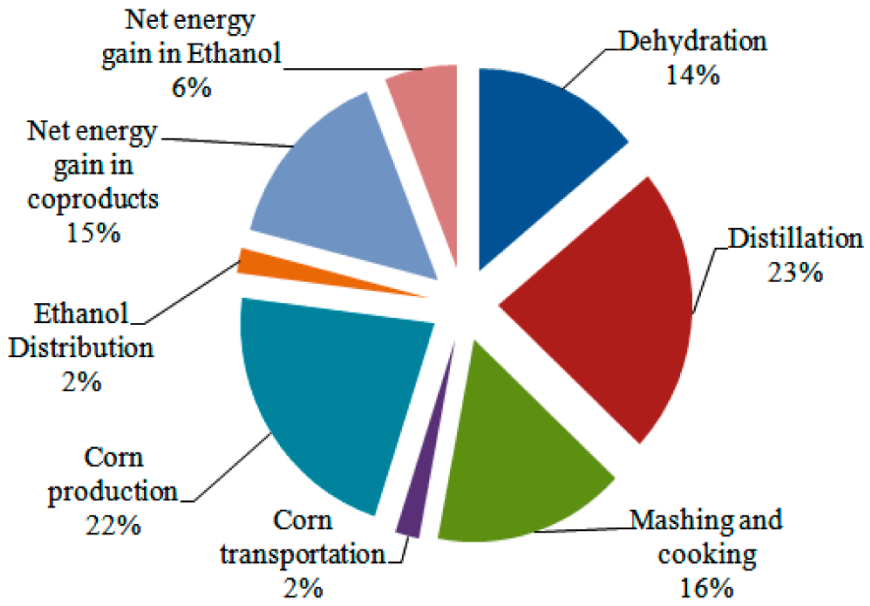

Figure 1.1 Net energy balance from corn ethanol manufacturing based on the study of Shapouri et al. [5]. The full circle represents the energy output of ethanol and co-products.

1.3 Part I: Research objective

- The goal of this study was to provide a comprehensive assessment of the thermophysical properties of hydrous ethanol-gasoline blends to examine their potential as a fuel blend for conventional SI engines.
- The fuel properties of hydrous ethanol-gasoline blends (H10, H15 and H30), anhydrous-ethanol gasoline blends (E10, E15 and E30), and pure gasoline (E0) were compared to ASTM D4814 [11], the standard specification for automotive spark ignition engine fuel to determine the feasibility of replacing gasoline with hydrous alternative fuels without requiring significant changes to current engine design and fuel delivery infrastructure.
- The evaporation of anhydrous with hydrous ethanol gasoline blends were compared by using distillation techniques and a droplet evaporation model to better understand how the

presence of water with its stronger azeotropic effect can affect the droplet evaporation dynamics.

1.4 Part II: Dual-alcohol blending approach

While the use of a neat alcohol as a fuel for spark-ignition engines would displace large amounts of petroleum, neat alcohols cannot provide the distillation temperature range required for smooth drivability and often exhibit high enthalpies of vaporization and low vapor pressures, which create cold-start problems. Even gasoline blends containing high concentrations of single alcohols have shortfalls. Blends of lower alcohols (methanol and ethanol) exhibit azeotropic behavior, lower calorific value, and low stability, while the low volatility of higher alcohols (C3 or higher) significantly limits the maximum fraction at which they can be blended.

One way to circumvent these issues is to use a dual-alcohol approach. Andersen et al. [12] discussed that it is possible to obtain an alcohol gasoline blend with a Reid vapor pressure (RVP) matching that of the base-gasoline by mixing a lower alcohol and a higher alcohol (ethanol and 1-butanol) in gasoline. A few studies have been conducted to test dual-alcohol blends using this approach. Siwale et al. [13] compared M70 (methanol 70 vol%+ gasoline 30 vol%) with a blend containing 53 vol% methanol, 17 vol% n-butanol and 30 vol% gasoline. The dual-alcohol blend was recommended in preference to M70 due to the shortened combustion duration, better volumetric efficiency, higher energy content, and better brake thermal efficiency while the RVP was selectively matched to that of gasoline. Ratcliff et al. [14] compared four blends with 5.5 wt % oxygen including a dual-alcohol blend (12% i-butanol-7% ethanol) and three single alcohol gasoline blends (16 vol % ethanol, 17 vol % n-butanol, and 21 vol% i-butanol) to study their effects on light-duty vehicle exhaust emissions. The dual-alcohol blend's exhaust emissions showed the lowest NOx, non-methane organic gas and unburned alcohols.

1.5 Part II: Research objective

- The primary objective of this study was to characterize the volatility behavior and evaporation limited mixing potential of dual-alcohol blends at a wide range of blending ratios.
- For this purpose, neat gasoline, three ethanol blends, and six dual-alcohol blends at blending ratios of 10, 20 and 40 vol % were prepared and characterized. Iso-butanol and 3-methyl-3-pentanol were used as the higher alcohols. These compounds were blended with ethanol and gasoline to match the RVP of the neat gasoline.
- The volatility behavior and mixing/sooting potential of the dual-alcohol blends were compared to the corresponding single alcohol blends (ethanol) using results from advanced distillation curve measurements and droplet evaporation models.

2 Literature Review

2.1 Background

For the past two centuries, the transportation sector mostly counts on fossil fuels (primarily petroleum) to derive mechanical energy from combustion of hydrocarbon fuels [15]. Gasoline, with 4–10 carbon atoms per molecule; jet fuel, with 10–14 carbon atoms per molecule; and diesel, with around 15– 22 carbon atoms per molecule, are the most common transportation and are derived from different cuts within the distillation column of a petroleum refinery [16]. Although low cost production and high energy density of fossil fuels make them the most cost-effective system for now and the near future, these resources are finite and unevenly distributed around the world. The ever-increasing demand for energy and uncertainty for petroleum supply results in fluctuations in oil price [4]. Furthermore, there are environmental issues associated with using fossil fuels such as greenhouse gas emissions, air pollution, and acid rain. These consequences adversely affect food, water resources, ecosystems, and other factors of the environment [15]. The depleting petroleum reserve, energy crisis, and global warming are reigniting the enthusiasm for seeking renewable and sustainable sources of energy [1]. Renewable energy sources include hydropower, wind, solar, geothermal, marine, and biofuel energy. In contrast to fossil and nuclear sources, the distribution of renewable energy resources is almost even around the world [17].

2.2 Biofuels

Among renewable energy sources, biofuels have the capability to replace a substantial fraction of fossil fuels especially for transportation applications [18]. In the United States, the Renewable Fuel Standard (RFS) which is created by the U.S. Environmental Protection Agency (EPA) sets levels of renewable fuel volume requirements to reduce greenhouse gas emissions and improve energy security. It calls to produce 36 billion gallons of biofuels annually by 2022, with

21 billion gallons coming from non-corn ethanol [2]. Producing drop-in biofuels which match all the standard fuel properties and are similar to petroleum-based transportation fuels would allow the use of existing engines while preventing huge amount of capital investments required for replacing the current fuel delivery infrastructure [19]. In addition, use of renewable oxygenates not only can address environmental issues, but also provide societal contribution such as employment in the agricultural sector [20].

Depending on the type of feedstock, different technologies can be exploited to convert biomass to biofuel [21]. Bioalcohols, biodiesel, bio-oils, bio-ethers, bio-esters, and synthetic hydrocarbons are the main types of biofuels. Among biofuels, biodiesel and bioalcohols are broadly commercialized and bio-esters have recently become an attractive fuel blend option [22]. First-generation biofuels include ethanol from corn and biodiesel from soybean or other edible oils [23]. The technology for production of first-generation biofuels is well-established with very high yield. However, there are increasing concerns over the environmental impacts, economic challenges, and food versus fuel issues [24]. These concerns have motivated efforts to find other feedstocks which are not dependent on agricultural resources that are commonly used for food, as is the case for corn and soybean [19]. Lignocellulosic biomass is non-edible and the most abundant biopolymer on the earth [19] composed of cellulose, hemicellulose, and lignin [25]. Fuels derived from lignocellulosic biomass are commonly termed second-generation biofuels [26]. Recently, new biosynthetic pathways have been engineered to produce new fuel molecules besides ethanol such as methanol [27], butanol [28], longer-chain alcohols [29], furan-based molecules, and bio-derived synthetic hydrocarbons [30]. However, cost-effective and energy-efficient processes to convert lignocellulose into fuels have not been established yet [19]. Third generation biofuel refers to fuels (mainly biodiesel) that are derived from algae feedstocks [23]. Since algae obtain their

energy from the sun during the photosynthesis process, algal biofuels can be thought of as natural batteries for storing solar energy while sequestering CO_2 [31]. To successfully commercialize the biofuel production, it is essential to have an integrative approach toward agricultural practice, land-use policy, water resource distribution, infrastructure of fuel distribution and usage, environmental evaluation, and technical aspects of biological conversion [24]. Among the alternatives, the two classes of biofuels currently receiving attention are biodiesels for blending with diesel and alcohols for blending with gasoline. These biofuels are more like fossil fuels than they are different, but the effects of even small differences must be investigated on engine performance and emissions [16].

2.3 Bio-derived anti-pollution and octane enhancer additives

The major transportation-related emissions are: oxides of nitrogen (NO_x), particulate matter (PM or soot), unburned hydrocarbons (UHC), carbon monoxide (CO), carbon dioxide (CO_2), and oxygenates such as aldehydes [23]. NO_x emissions can cause acid rain which result in acidification of lakes and streams. In addition, NO_x can react with volatile organic compounds (VOCs) to form ozone which is a major cause of urban smog [32]. Soot emissions are particularly damaging when their size is below 10 μm which can penetrate deeper into the lungs causing serious health issues [23]. Carbon monoxide at adequately high levels can be deadly by reducing the oxygen-carrying capacity of the blood. Carbon dioxide emission is also important due to its greenhouse effect and depends on engine power output and efficiency, and the hydrogen-to-carbon ratio of the fuel [23]. Oxygenated emissions, especially aldehydes and ketones, are toxic but unregulated emissions that must be considered [33]. Polycyclic aromatic hydrocarbons known as PHA are also very toxic pollutants that can cause cancer and contribute to the formation of secondary particulate matter [34].

For a long time, the key motivation for advancements in engine technologies has been the increasingly-strict exhaust-emission regulations and fuel economy standards forced to enhance air quality and human health. Given the increasingly stringent emissions standards, it is vital to have a combined approach toward production of high efficient engines and use of alternative low-emissions-producing fuels to meet air quality regulations.

Accordingly, refineries have strived to reduce the contribution of their fuel to harmful exhaust emissions [35]. A high octane number is desired to avoid engine knocking, but not all octane enhancers are environmentally-friendly. For instance, lead is an octane booster, but lead additives are toxic air pollutants and poison the catalysts in the exhaust system and have been outlawed 1975. When unleaded gasoline became a mandate, petroleum refineries tried to add other additives to keep the octane number high enough. The other option was aromatics such as benzene and toluene, but these are known as carcinogenic compounds and contributors to more smoke and smog. In addition, use of high concentration of olefins was also rejected because it results in deposits/gum formation and an increase in emission of ozone forming hydrocarbons and toxic compounds [20]. Eventually, oxygenates produced from renewable resources have been proposed as gasoline blend additives to simultaneously increase the knock resistance and reduce exhausts emissions. Oxygenates can effectively reduce the CO, CO_2, UHC and soot emissions. However, it is worth noting that the reduction in emission is not solely controlled by the oxygen mass fraction because oxygenates with different functional groups (alcohols, ethers, esters, and ketones) can have different results [36].

In the United States, Clean Air Act amendments of 1990 mandate the use of reformulated and oxygenated gasoline in order to decrease emissions [37]. Initially, Methyl tert-butyl ether

(MTBE) and Ethyl tert-butyl ether (ETBE) had been used. However, they were prohibited shortly after due to the water contamination and were replaced mainly by ethanol [35].

2.4 Alcohols as alternative biofuels

Alcohols are organic compounds with one or more hydroxyl group(s). Mono-alcohols, which are alcohols with only one hydroxyl group (OH), are classified as primary, secondary, and tertiary based on the location of hydroxyl group in the molecular structure. In primary, secondary and tertiary alcohols, the OH group is attached to a carbon bonded to one, two, and three alkyl group(s), respectively.

The "substantially similar" rule published by EPA stated that alcohols can be blended with gasoline up to oxygen content of 3.7 mass % [38]. Alcohols are particularly attractive and the influence of alcohol blends with gasoline on performance and emissions in spark ignition (SI) engine has been largely investigated [39]. The technology for production of alcohols is available and well established primarily for methanol and ethanol. Methanol can be produced from coal, biomass, and natural gas [40]. Ethanol can be produced biologically by fermentation of sugars and starch [39] and the non-sugar fraction of lignocellulosic biomass. Ethanol is also produced chemically through direct hydration of ethylene and the Fischer–Tropsch process (catalytic conversion of syngas to a mixture of alcohols) [20]. In the case of higher alcohols (alcohols with higher molecular weight than ethanol), economic and environmentally-friendly methods have not been established yet. Conventionally, higher alcohols are produced from coal derived syngas which is not environmentally-friendly because coal is not a clean/renewable source of energy [35]. The alternative is to produce syngas from sustainable and renewable feedstocks and then catalytically convert the biomass-waste derived syngas to produce a mixture of methanol, ethanol and a small fraction of other higher alcohols. Moreover, higher alcohols can be naturally produced

from some species such as clostridia via fermentation. However, the efficiency of industrial fermentation is currently low and recently many research studies have been conducted to engineer microorganisms to produce higher alcohols [15].

In the United States, ethanol has been used in gasoline blends to improve the octane rating because of well-established and low-cost production processes [23]. Currently, the use of gasoline blends containing up to 15 vol % in vehicles model year 2001or newer is allowed [41]. However, there are some modifications required for the best use of blends containing high fraction of lower alcohol in conventional SI engine which are not optimized for these alcohols because they are strong solvents and highly corrosive to some metal parts of the engines. One option is to redesign the engines and infrastructures to be compatible with alcohols. However, the capital cost associated with this approach is prohibitively high. The other option is to use additives to improve the blend's characteristics [20]. In addition, lower alcohols suffer from some drawbacks such as low energy density, azeotropic behavior, low stability [20], and high hygroscopicity [15]. In contrast, higher alcohols offer higher energy density [14], low or no azeotropic behavior [42], lower water affinity, higher stability [43], and more compatibility with current system due to their similarity to gasoline [14]. Hence, use of higher alcohols as co-solvents can offset shortcomings associated with lower alcohol blends.

2.5 Spark-ignition engine

A brief description of spark-ignition (SI) engines and effect of using alcohol biofuels in these engines will be discussed in the following sections. In conventional port-fuel-injection (PFI) engines, fuel is pre-vaporized and well mixed with the air in the intake manifold prior to the cylinder. The premixed air-fuel mixture is then ignited by a spark plug located inside the cylinder at the desired time during the piston's cycle of motion. As a result, a high-temperature turbulent

premixed flame is generated which propagates through the well-mixed fuel–air charge [44]. The fuel–air ratio must be kept as close as possible to the stoichiometric fuel–air mixture to avoid oxygen in the exhaust system to ensure the best use of the 3-way catalyst needed for exhaust treatment [45]. However, at the stoichiometric fuel–air ratio, the flame temperature is high leading to high NO_x and added propensity for knock.

Conventional PFI SI engines have some shortfalls such as pressure drop across the throttling valve, limited compression ratio (CR) due to the knock possibility, and the high level of NO_x emissions [46]. Thus, the idea of direct-injection spark-ignition (DISI) engines was generated to enhance the thermal efficiency and fuel economy by eliminating the throttle valve and controlling the engine power via varying the amount of fuel injected directly into the engine cylinder per cycle [47]. These modifications make the engine more fuel flexible and allow a higher compression ratio to be used because the fuel is vaporized within the cylinder leading to the charge cooling and a reduced knocking potential [23]. The fuel economy is claimed to be 20–25% better than PFI systems [48]. High pressure fueling systems are used in DISI engines to provide finer atomization which contributes to better evaporation and mixing [44]. However, mixing is limited compared to PFI systems and the resultant air-fuel mixture can be stratified with high fuel-concentrations near the spark plug which generally results in higher fuel impingement on cylinder walls, soot, UHC and NO_x emissions even after considering the charge cooling effect [48].

2.5.1 General effects of alcohols on SI engine performance

The heat of vaporization (HoV) of alcohols (especially lower alcohols) is higher than that of gasoline. In direct injection systems, the required energy for evaporation is supplied from the intake air and cylinder walls causing a charge cooling effect and reducing compression work. In PFI systems, high HoV lowers the temperature in the intake manifold increasing the amount of

fuel mass in the cylinder. These properties of alcohols can lead to a better thermal efficiency compared to neat gasoline especially in consideration of the high octane rating of these fuels which allows application of high compression ratios [49]. Since SI engines must run at stoichiometric ratio, more neat alcohol or blend of alcohols must be injected in each power cycle in comparison to gasoline. However, it is difficult to evaluate the alcohol's influence on brake specific fuel consumption (BSFC) because although the heating value of alcohols are lower than gasoline, more complete combustion due to the oxygen content, faster flame speed, higher HoV, and higher octane rating may lead to higher power-output with alcohol fuels [50].

Since the stoichiometric air–fuel ratios of alcohols are lower than gasoline, lower amount of air is required for a complete combustion. In addition, oxygen content of alcohols eases oxidation of CO into CO_2. Hence, given the lower number of carbons in alcohols, the levels of CO and CO_2 emissions are usually lower relative to gasoline. In addition, more complete combustion of alcohols can contribute to lower unburned hydrocarbons (UHC) production. However, high HoV may cause misfire or partial burn in the regions near the cylinder wall under certain conditions and increases UHC emissions [39, 42].

Results for effect of alcohols on NOx production are mixed. Some studies reported a reduction in NO_x because of charge cooling effect of alcohols [51, 23] while others reported increased NO_x emissions due to the more complete combustion, higher heat release, faster flame speed, and higher compression ratios that are used [39].

In general, alcohols as fuel additives can reduce the amount of PM in the exhaust system. The role of the specific structure of the oxygenate molecule is still a question, but generally it is stated that oxygenated molecules isolates the bonded carbon which reduces the number of carbon atoms that are active in the radical pool for the formation of soot precursors. It is proven that fuel

composition has the most important effect on soot formation [52], but other factors such as HoV, ignition property, boiling characteristics, and viscosity also play significant roles in soot formation [53]. For instance, high heat of vaporization of alcohols retards the evaporation of the fuel inside the chamber in direct injection systems. Thus, at higher speeds of engine there may not be enough time for fuel droplets to completely evaporate which could result fuel pooling on cylinder/piston surfaces and inhomogeneous surface combustion phenomenon which results in soot emissions [25]. Use of alcohols in gasoline blends could change combustion pathways toward production of oxygenates such as formaldehyde, acetaldehyde and ketones as result of partial oxidation of alcohols. Potential increase in oxygenated emission is an important concern that must be addressed although these are not regulated emissions [54].

2.5.2 General effects of hydrous ethanol on SI engine performance

Although hydrous ethanol may cause negative long-term impacts such as lubricant deterioration and fuel system corrosion [8], its overall impact on combustion and emission characteristics has been shown to be positive. Schifter et al. [55] compared exhaust emissions and engine performance of gasoline blended fuels containing 10 to 40 % by volume of hydrous ethanol (4 vol % water + 96 vol % ethanol) to those of gasoline-anhydrous ethanol blends with the same ratios in a single cylinder port fuel injection spark ignition (SI) engine with equivalence ratio varying from 0.9 to 1.1. Their general observation suggests that presence of water is more important than the amount of water. Intake temperature was decreased with the presence of water due to the high HoV of water. However, the intake temperature was not changed notably with further increase in concentrations of water. Results showed that the increase in water content decreased the NO_x emissions as a result of reduced peak combustion temperature but also increased the fuel consumption due to the lower calorific value of the hydrous blends. The effect of water on

the octane value quantity was negligible although Cooperative Fuel Research (CFR) engines are highly sensitive to the fuel's charge cooling [56]. In terms of thermal efficiency, the hydrous ethanol blends performed almost identically to the anhydrous ethanol blends. Authors credited this observation to the higher charge cooling effects of hydrous blends which compensates for their slower combustion process and lower heating value.

Kyriakides et al. [57] compared a specific mixture of 60:30:10 gasoline: ethanol: water (E40h) to an ethanol-gasoline blend (E40) in an Otto engine. Similar to the results of Schifter et al. [6], they reported a significant reduction in NO_x and an increase in fuel consumption with E40h. In addition, no difference in engine torque was noticed between E40 and E40h. Costa and Sodré [58] used a fuel flexible engine to compare neat hydrous ethanol (6.8 vol % water + 93.2 vol % ethanol) with an ethanol-gasoline blend (E22). In terms of emissions, hydrous ethanol produced lower level of CO and unburned hydrocarbons (UHC) emissions than E22, but higher CO_2 and NO_x. The increase in NO_x was attributed to the faster flame speed and the use of more advanced ignition timing for the hydrous ethanol fuel, which both favor the production of higher peak temperatures. Hydrous ethanol showed a higher thermal efficiency compared to E22 which was explained by reduced heat loss to cylinder walls due to the higher HoV and faster flame speed of the hydrous ethanol. However, the lower heating value of hydrous ethanol led to an increase in brake specific fuel consumption (BSFC). Hydrous ethanol produced lower torque and brake mean effective pressure (BMEP) at low engine speeds (below 3250 rpm), with the trend inversed at higher speeds (over 4000 rpm). To justify this behavior, authors stated that since there is enough time for complete combustion at low engine speeds, the lower heating value is the dominant factor. However, faster flame velocity is favorable at higher engine speeds due to the limited time for a complete combustion. Melo et al. [59] studied combustion and emission characteristic of gasoline

blends with hydrous ethanol at different ratios operating in a 1.4 L, Flex-Fuel Otto engine. In this study, E25 (25 vol. % anhydrous ethanol+ 75 vol. % gasoline) was used as a base fuel and subsequently was blended with 30, 50, 80 and 100 vol. % of hydrous ethanol (H30, H50, H80 and H100). The hydrous ethanol contained 4.3 vol. % of water to match the azeotrope proportions. In general, blends with higher ethanol content showed higher BSFC and CO_2 while lower CO and UHC. Results of NO_x showed complex trends with ethanol addition and were highly dependent on the operating conditions.

Wang et al. [60] compared combustion and emission characteristics of pure gasoline, anhydrous ethanol-gasoline blend (E10), and hydrous ethanol (H10) operating in a port injection gasoline engine. In this study, hydrous ethanol contained 5% water by volume. Gasoline exhibited the highest peak pressure at the low and medium loads followed by H10 and E10, respectively, while at high load H10 produced the highest peak in-cylinder pressure. This behavior has its roots in the high HoV of ethanol which decreases combustion temperatures, leading to a lower peak in-cylinder pressure at low and medium loads; however, the negative effect of high HoV diminished at higher loads. The peak heat release rates of H10 were higher than both gasoline and E10 at all the tested operating conditions. At low and medium loads, the peak heat release rates of gasoline were higher than E10 while at high load the peak heat release rates of E10 were higher than those of gasoline. These behaviors were justified with the same rationale for peak in-cylinder pressure. Ethanol addition increased NO_x emissions especially at high load. Authors stated that relative oxygen-enrichment in the reaction regions and a faster flame propagation and combustion process which results in a higher temperature in the cylinder are reasons for this increase. The increase in NO_x emission was slightly lower for H10 in comparison to E10 because the HoV of water is higher than ethanol leading to a stronger cooling effect. Presence of oxygen in both hydrous and

anhydrous ethanol blends caused less CO and UHC emissions compared to gasoline especially at low and medium loads. The level of CO and UHC emissions at low and medium loads for H10 was greater than E10 which can be attributed to higher charge cooling effect of water slowing the oxidation kinetics of CO and unburned hydrocarbons.

All previous studies conducted on hydrous ethanol are limited to engine behaviors such as fuel consumption, engine efficiency, BMEP, and exhaust emissions. Following a review of these studies, in general, negligible differences in fuel economy, engine performance, and emissions were observed when comparing hydrous and anhydrous ethanol blended fuels. Furthermore, it should also be noted that the engines used in these previous works were stock and were not tuned to operate on higher ethanol concentrations with water. Tuning engine parameters related to the compression ratio, injector design, boost pressure, along with spark and valve timing could lead to the realization of better performance with the hydrous ethanol fuels.

3 Experimental and numerical methods

3.1 Introduction

In this chapter, the experimental and numerical methods exploited in Part I (hydrous ethanol-gasoline mixtures) and Part II (dual-alcohol blending approach) are explained. The list of blends and their preparation methods for each part will be explained later in their corresponding chapters. In both collaborative projects, my duties included carrying out distillation measurements, including distillate sampling and chemical composition analysis of the samples, and running the distillation curve and droplet evaporation models. In addition, I had some contributions to characterization tests including Reid vapor pressure, vapor lock index, viscosity, density, copper strip corrosion, haze and phase separation points, and lower heating value.

3.2 Test fuels

In this study, unleaded test gasoline (UTG-96) from Phillips 66 was used as the base fuel to which the alcohol compounds were blended with (more specifications are available in [61]). Ethanol (200 proof, ≥ 99.5%) was purchased from Pharmco-AAPER. Iso-butanol (≥ 99 %, FG) and 3-methyl-3-pentanol (≥ 99 %, FG) were obtained from Sigma-Aldrich. All test fuels were stored in a freezer at -18 °C to avoid errors stemming from unintentional evaporation.

3.3 Experimental methods

3.3.1 Characterization tests

Fuel characterization is the primary step in the evaluation of any for a combustion process. In these studies, fuel characterization includes viscosity, density, copper strip corrosion, haze and phase separation points, water tolerance, and lower heating value. An Anton Paar SVM 3000 viscometer- densitometer with repeatability of 0.35% for viscosity and 0.0005 g/cm^3 for density was used to measure viscosity and density of test fuels at 20 °C. Copper strip corrosion test was

conducted using a copper strip tester (Protest) based on ASTM D130-12 [62] to ensure that there would be no corrosion to fuel system metals due to reactive sulfur compounds in the fuel and any possible corrosion which can be attributed to the alcohols. Phase separation temperature was determined with a Lawler cloud point DR4-14 (repeatability of ±1.13 °C) according to ASTM D 6422–99 to measure stability of water in ethanol-gasoline blends at different temperatures and concentrations of ethanol [63]. Lower heating value (LHV) was measured with an IKA C200 calorimeter according to ASTM D240-14 [64] with relative standard deviation of 0.1% to quantify the energy density of each test fuel.

3.3.2 Volatility measurements and composition analysis

Reid vapor pressure (RVP) is the vapor pressure exerted by a liquid fuel at 37.8 °C with a vapor-to-liquid ratio equal to 4:1. Vapor lock index is the temperature at which a fuel forms a volumetric vapor-liquid ratio of 20 and is used to address vapor lock problems. The RVP and the vapor lock index were measured using a Grabner Instruments Minivap VPXpert vapor pressure analyzer with repeatability of 0.3 kPa according to ASTM 5191 [65] and ASTM D5188 [66], respectively.

A custom-built Advanced Distillation Curve (ADC) apparatus was used to obtain the distillation curves [67- 69]. The schematic view of ADC is shown in Figure 3.1.

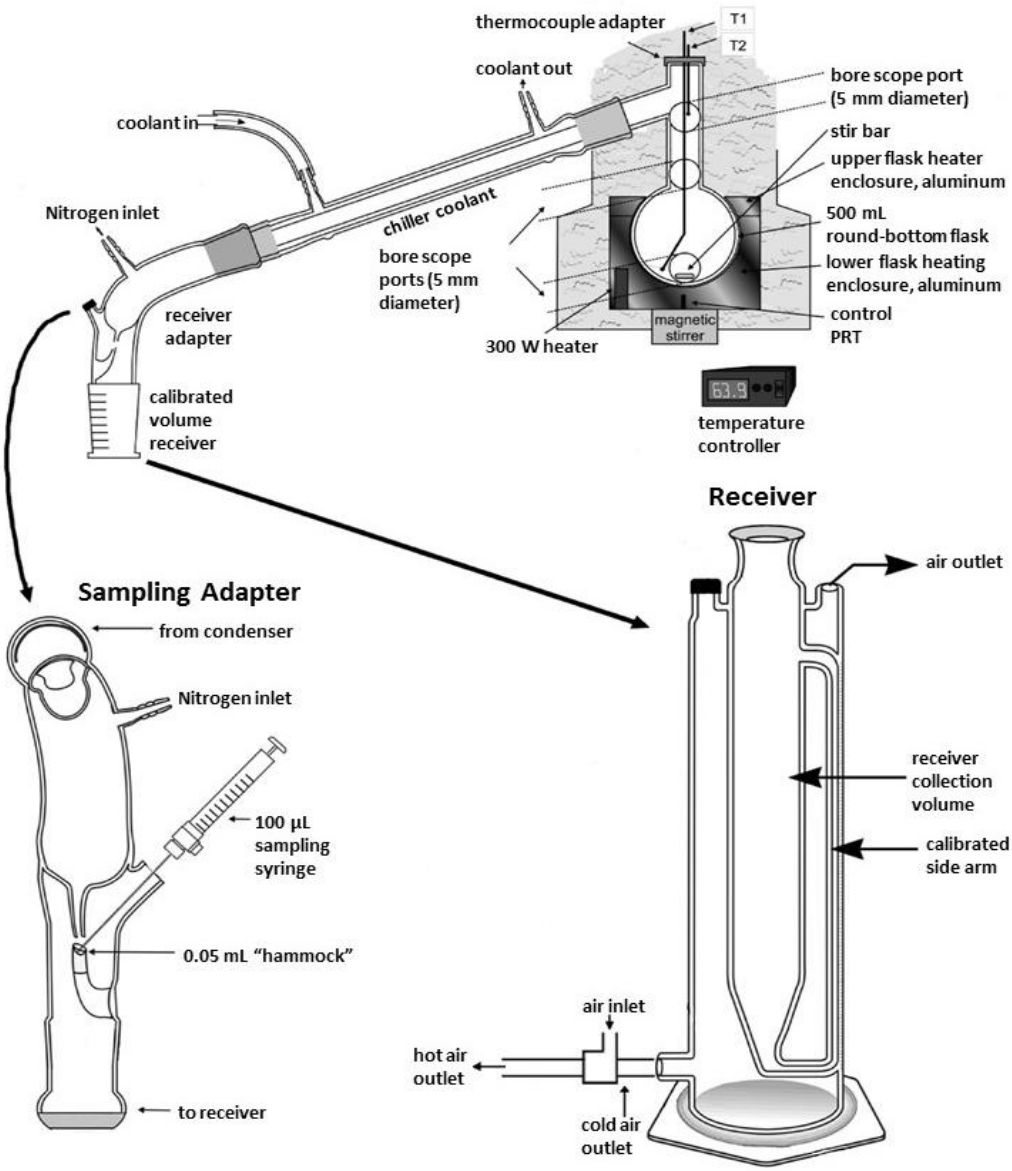

Figure 3.1 Advanced distillation curve apparatus [67]

Details of the ADC method have been widely reported elsewhere [70]. In brief, a temperature-controlled heating mantle is placed around the boiling kettle containing 200 ml of the fuel blend, which is stirred to ensure a uniform composition and temperature within the boiling mixture. Temperatures of the liquid in the kettle and vapor in the distillation head are monitored with two K-type thermocouples. These thermocouples continuously record temperatures using a data acquisition (DAQ) system. The temperature of the heating mantle is continuously adjusted to

lead the boiling fluid temperature by ~20°C ensuring even heating throughout the distillation process. The condenser tube is chilled with water maintained at 5°C. The apparatus is equipped with a custom sampling adapter located between the condenser tube and the volumetric receiver, which provides the ability to withdraw samples of the distillate during the distillation process. The volumetric receiver collects the condensed liquid and is calibrated to measure the distilled liquid volume. The receiver is cooled by chilled air from a vortex tube at 2°C to prevent any vapor loss. At every 5% volume distilled, the liquid temperature in the kettle is recorded and used to create an accurate distillation curve. Distillation curves for each mixture were measured twice to ensure repeatability. Generally, the initial boiling temperature (IBT) is difficult to observe and measure. In this study, the IBT corresponds to the temperature of the boiling liquid (in the kettle) at the point when a sudden rise in the head temperature was observed (or the point of maximum gradient during post-processing) like the methods suggested by Ferris and Rothamer [71]. To illustrate, Figure 3.2 shows liquid and vapor temperatures versus time for gasoline in which sudden rise in vapor temperature is shown with a red circle. In this method, IBP is identified based on minimum of the second derivative of vapor temperature with respect to time in the interval of 180 seconds before and 240 seconds after the first drop temperature.

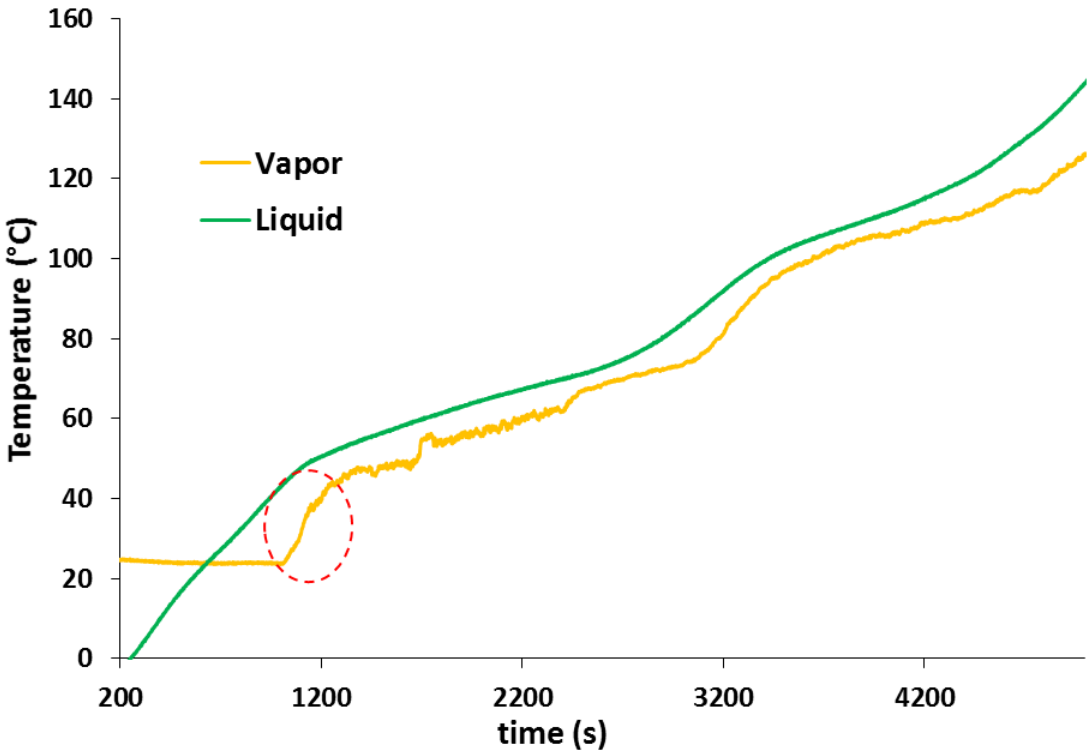

Figure 3.2. Liquid and vapor temperatures plotted versus time

Distillate samples were taken at the first drop, 10, 20, 30, 40, 50, 60, 70, 80 and 90% volume distilled. An HP 5890 Series II GC- FID was used to analyze the composition of the samples according to ASTM D6729 [72]. The GC was equipped with 100 m long Petrocol DH fused silica capillary column coated with polydimethyl siloxane. Species were identified by comparing peak retention times to those measured with reference standards. For the UTG-96 gasoline, it was noticed that the heavy fraction contained many species with small peak areas (or mass fraction). Though the individual species were a minor fraction of total composition, the integration of these peaks was found to be a significant portion of the fuel. To ensure for proper distribution of species and accurate prediction of distillation curves, a grouping approach was exploited to determine a simplified composition for the gasoline. To identify unknown hydrocarbons with excessively small chromatogram peak areas toward this approach assumed the small peaks to be of the same composition to the nearest known identified hydrocarbon peak. An

illustration of this approach is depicted in Figure 3.3. Here, Biphenyl and Hexylbenzene are two gasoline components with known retention times and relatively high peak areas. The small peaks between these compounds are lumped with Biphenyl (red box) at retention times before the midpoint (average retention times of these known compounds) and lumped with Hexylbenzene (green box) afterward. By lumping together species with similar molecular weight and physiochemical properties, this approach was able to simplify the complex composition of the gasoline to 54 compounds while maintaining a strong agreement between predicted and measured distillation curves (demonstrated later). Chromatogram peak areas were then converted to the mass concentrations following calibration. The chromatogram of the UTG-96 and a list of the simplified composition are provided in the Table 3.1 and Figure 3.3. To monitor the water evaporation, the water content of the distillate samples was measured by Karl Fischer titration using a Metrohm 831 KF coulometer. In this method, the sample taken from distillation is injected to the titration vessel where iodine is generated coulometrically at the anode for the Karl Fisher reaction. At the titration termination point, the excess iodine is detected via electrometric end-point detector. Then, the quantity of water is calculated proportionally based on the stoichiometry of the reaction.

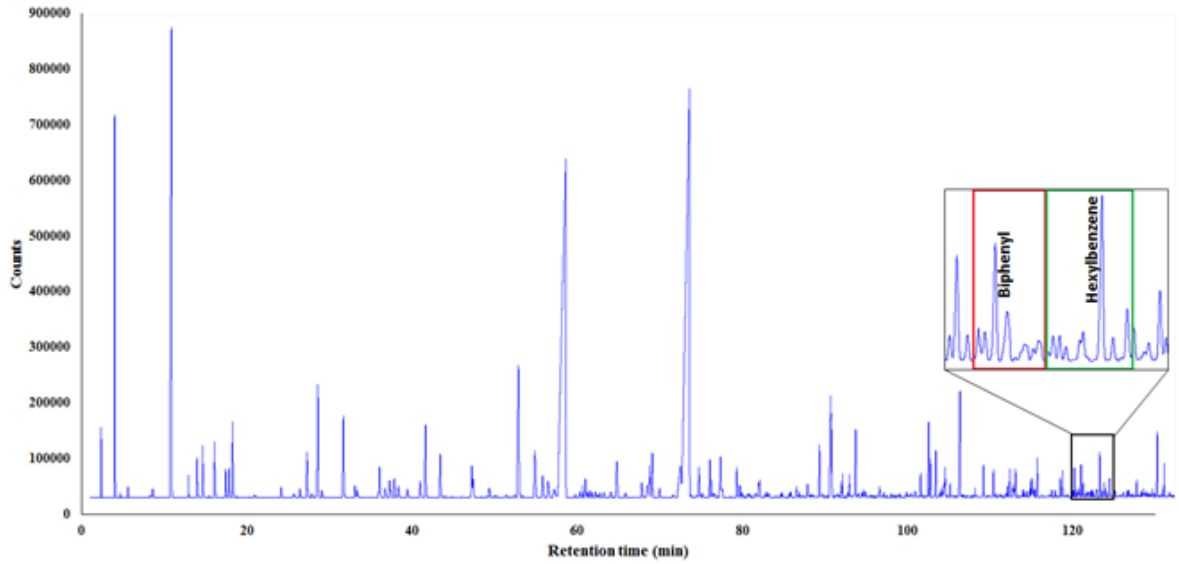

Figure 3.3 Gas Chromatogram of Gasoline

3.4 Distillation and droplet models

A distillation curve model, based on the work by Backhaus [73], was used to predict the distillation curve, changes in composition and HoV of the test fuels during distillation. In an ideal mixture, vapor-liquid equilibrium (VLE) can be obtained simply from Raoult's Law and Dalton's Law in which the activity coefficient (γ) is equal to unity as shown in equations 3.1 and 3.2.

$$p_i = y_i p_{tot} \quad \text{Eq.3.1}$$

$$p_i = \gamma_i x_i p_i^0 \quad \text{Eq.3.2}$$

Where pi is the partial vapor pressure of the component i, yi is the mole fraction of the component i in the gas phase, p_{tot} is the ambient pressure, γi is the activity coefficient of the component i, xi is the mole fraction of the component i in the liquid phase, and p_i^0 is the vapor pressure of the pure component i.

Table 3.1 Gasoline's detailed composition

Compound	Group	Mass fraction	Retention times
i-Butane	Isoparaffin	0.0055	10.79
n-Butane	Paraffin	0.0329	12.17
i-Pentane	Isoparaffin	0.0833	17.91
2-Methyl-1-butene	Olefine	0.0072	20.53
n-Pentane	Paraffin	0.0061	21.07
trans 2 pentene	Olefine	0.0067	22.24
Cis-2-pentene	Olefine	0.0037	23.32
2-methyl-2-butene	Olefine	0.0098	24.00
2,3-Dimethylbutane	Isoparaffin	0.0107	31.42
2-Methylpentane	Isoparaffin	0.0213	32.51
3-Methylpentane	Isoparaffin	0.0157	35.08
n-Hexane	Paraffin	0.0066	38.68
2-Methyl-2-penten	Olefine	0.0093	40.24
Methylcyclopentane	cycloalkane	0.0142	43.35
2,4-Dimethylpentane	Isoparaffin	0.0076	44.82
3-methyl Cyclopentene	cycloalkene	0.0044	48.09
Benzene	Aromatic	0.0054	48.24
2,3,dimethylPentane	Paraffin	0.0282	52.81
3-Methylhexane	Isoparaffin	0.0097	54.50
Cyclopentane, 1,3-dimethyl-, cis-	cycloalkane	0.0076	55.31
2,2,4-Trimethylpentane	Isoparaffin	0.2005	57.43
n-Heptane	Paraffin	0.0028	59.39
Cis-3-heptene	Olefine	0.0067	59.70
Methylcyclohexane	cycloalkane	0.0100	62.92
2,3,3-Trimethylpentane	Isoparaffin	0.0103	66.28
2,4-Dimethylhexane	Isoparaffin	0.0087	66.59
2,3,4-Trimethylpentane	Isoparaffin	0.0245	69.38
Toluene	Aromatic	0.2166	70.23
2,3-Dimethylhexane	Isoparaffin	0.0051	71.40
2-Methylheptane	Isoparaffin	0.0074	72.53
3-Methylheptane	Isoparaffin	0.0086	73.71
1-methyl-1-ethylcyclopentane	cycloalkane	0.0062	75.41
2,2,5-trimethylhexane	Aromatic	0.0091	77.69
Ethylbenzene	Aromatic	0.0132	84.00
p-Xylene	Aromatic	0.0162	85.14
2-methyl-Octane	Paraffin	0.0066	85.25
3-Methyloctane	Isoparaffin	0.0052	86.29
1-nonene	Olefine	0.0180	87.80
1 ethyl-2 methyl benzene	Aromatic	0.0191	95.43
1,2,4-trimethylbenzene	Aromatic	0.0112	96.19
1,2,3-trimethylbenzene	Aromatic	0.0172	98.66
1,4-diethylbenzene	Aromatic	0.0049	101.19
C10 aromatic	Aromatic	0.0039	102.24
2-ethyl-1,4-dimethyl	Aromatic	0.0043	103.93
C11-paraffin	Paraffin	0.0062	104.50
C11-aromatic	Aromatic	0.0102	106.78
1,2,3,4-tetrahydronaphthalene	Aromatic	0.0035	109.25
Naphthalene	Aromatic	0.0025	109.50
n-Dodecane	Paraffin	0.0035	110.71
Biphenyl	Aromatic	0.0070	111.41
Hexylbenzene	Aromatic	0.0117	113.33
Hexamethylbenzene	Aromatic	0.0074	117.27
2,6-dimethylnaphthalene	Aromatic	0.0073	119.37
Acenaphthalene	Aromatic	0.0084	120.12

The equilibrium ratio is defined as the ratio of molar fraction of each species in vapor to its molar fraction in the liquid.

$$K_i = \frac{y_i}{x_i} = \frac{\gamma_i p_i^0}{p_{tot}} \quad \text{Eq.3.3}$$

To calculate the VLE of gasoline blends with oxygenates which exhibit non-ideal behavior, the non-unity gamma term should be calculated. In case of non-ideal mixtures, the γ_i is defined as the ratio of the actual vapor pressure of each species to its ideal vapor pressure. In this distillation model [73], the activity coefficient is calculated with the UNIFAC group contribution method. This theory consists of two components known as combinatorial (γ_c) and residual (γ_r) as shown in Eq. 3.4.

$$\ln \gamma = \ln \gamma_c + \ln \gamma_r \quad \text{Eq. 3.4}$$

The combinatorial component describes the geometric interaction between molecules while the residual component is a function of polarity and temperature.

The inputs for both the distillation and droplet evaporation models are the initial compositions of each blend, the ambient pressure and am initial temperature. In the distillation model, the first step is to predict evolving composition of the liquid before temperature curves can be calculated. The change in the liquid composition can be calculated as a function of the instantaneous vapor composition by following equation:

$$\frac{dx_i}{dL} = \frac{(K_i - 1)x_i}{L} \quad \text{Eq.3.5}$$

Where L is the fraction of total moles in the system that are in the liquid state and K_i is the equilibrium ratio. This ordinary differential equation is integrated in small intervals from L=1 to L=0 to obtain the composition during the distillation. Then, to obtain the temperature at each VLE, the model exploits a Newton-Raphson method iterating on the liquid temperature and calculating the equilibrium compositions until the sum of each species' partial pressure equals the ambient

pressure. This method starts with a given temperature (usually 350 K) and iterates until a tolerance of 0.1 mPa is obtained.

As discussed, distillation model works only based on liquid composition. However, the droplet model must incorporate time, energy, and mass. Burke et al. [74] modified Backhaus's model to simulate the distillation process in a droplet by incorporating the D^2 law and appropriate energy and mass transfer dynamics. To predict evaporation time, mass flux with respect to time is calculated by the following equation:

$$\frac{dm}{dt} = \dot{m} = 4\pi r_s \rho_{vap} D_{FA} \ln\left(\frac{1}{1-Y_F}\right) \quad \text{Eq. 3.6}$$

Where:

- r_s= current droplet radius
- ρ_{vap}= vapor density (calculated as an ideal gas)
- D_{FA} = diffusivity coefficient estimated using a molecular weight-based approximation for hydrocarbons
- Y_F = the vapor mass fraction of fuel at the droplet interface

In addition, changes in temperature of the droplet with respect to time was derived from an energy balance of the internal sensible heat of the droplet, heat of vaporization in combination with droplet mass flux, and heat conduction from the surroundings to the droplet as shown in Eq. 3.7.

$$\frac{dT}{dt} = \frac{-\dot{Q}_{cond} - \dot{m} h_{fg}}{m_{drop} c_{p,liq}} \quad \text{Eq. 3.7}$$

In this study, the distillation curve model was validated with the experimental distillation curve and distillate composition data and the droplet evaporation model was used to predict evaporation time for the test blends under different temperatures and droplet size conditions. The droplet evaporation model was used to infer the potential of oxygenate addition on PM formation

due to depressed droplet evaporation rates stemming from charge cooling effects and aromatic enrichment as described in [70]. Mixture properties including the HoV were determined using a mass fraction weighted average approach as described in [75].

4 Azeotropic Volatility Behavior and Physiochemical Property Characterization of Hydrous and Anhydrous Ethanol Gasoline Mixtures

4.1 Background

Water removal during the production of bio-ethanol obtained from fermentation is highly energy intensive. At the azeotrope point, the mixture can no longer be separated via fractional distillation requiring expensive and energy intensive methods for further purification. Hence, there is an interest in using hydrous ethanol at the azeotrope point to improve the energy balance of ethanol fuel production.

There has not been a comprehensive study to characterize the thermophysical properties of hydrous ethanol gasoline blends to examine its potential as a fuel blend for conventional spark ignition engines. This study compares the fuel properties of hydrous ethanol-gasoline blends, anhydrous-ethanol gasoline blends and pure gasoline. Experimental results were compared to standard specification for automotive spark ignition engine fuel-ASTM D4814 [11] to determine the feasibility of replacing gasoline with hydrous alternative fuels without requiring significant changes to current engine design and fuel delivery infrastructure. In addition, this study intended to explore the complex azeotropic effect on volatility of anhydrous and hydrous ethanol blends to gain a better understanding of evaporation behavior and the role of water and its stronger azeotropic effect on droplet evaporation dynamics. To achieve this goal, an advanced distillation apparatus was used to obtain distillation curves for gasoline, gasoline-hydrous ethanol and gasoline-anhydrous ethanol mixtures. Distillate samples were withdrawn at various points during distillation and their corresponding compositions were quantified, including the transient distillate water concentration. A distillation-based droplet evaporation model validated with the

experimental data was used to help explain volatility differences between the hydrous an anhydrous fuel and provide insight into their PM formation potential.

4.2 Test fuels

In this study, unleaded test gasoline (UTG-96) from Phillips 66 was used as a reference fuel identified as E0. The detailed composition of gasoline obtained in this study is available in the Table 3.1. Ethanol (200 proof, ≥ 99.5%) was purchased from Pharmco-AAPER. Gasoline was blended by volume with 10%, 15% and 30% of anhydrous and hydrous ethanol referred to hereinafter as E10, E15, E30, H10, H15, and H30. Hydrous ethanol was prepared by blending 96 vol. % of anhydrous ethanol with 4 vol. % of deionized water. All test fuels were stored in a freezer at -18 °C to avoid errors because of unintentional evaporation. Blends containing 10% and 15% ethanol were selected because they are the common ethanol concentrations in use today and currently maximum allowable ethanol concentration in the US market. Blends consisting of 30% ethanol were also considered to study the effect of higher concentration of ethanol and water content on fuel specifications.

4.3 Results and discussion

The complete set of characterization data for all test fuels are given in Table 4.1. Subsequent discussion will comment on relative differences between the test fuels and the impact of these on fuel usability.

Table 4.1 Properties of test fuels. Error ranges correspond to +/- standard deviation.

Property	Gasoline (E0)	E10	E15	E30	H10	H15	H30
Ethanol content (vol %)	0	10	15	30	9.6	14.4	28.8
Water content (vol %)	0	0	0	0	0.4	0.6	1.2
Reid vapor pressure (kPa)	53.13 ± 0.16	59.54 ± 0.28	59.26 ± 0.17	55.03 ± 0.18	61.36 ± 0.86	61.49 ± 0.57	57.88 ± 1.16
$T_{v/l=20}$ (°C)	66.33 ± 0.34	57.2 3± 0.41	58.8 ± 2.77	58.63 ± 0.28	55.4 ± 0.08	55.5 ± 0.3	57.67 ± 0.05
Initial boiling point (°C) at 84 kPa	48.4 ± 0.5	48.45 ± 0.93	48.6 ± 0.59	49.3 ± 0.88	48.62 ± 0.32	48.66 ± 0.41	48.85 ± 1
T10 (°C) at 84 kPa	70.71 ± 0.49	59.60 ± 0.83	59.67 ± 0.79	61.25 ± 0.74	59.28 ± 0.94	58.59 ± 0.93	59.8 ± 0.86
T50 (°C) at 84 kPa	103.08 ± 0.72	102.13 ± 0.79	81.51 ± 3.91	73.16 ± 0.03	102.72 ± 1.43	85.58 ± 1.16	71.93 ± 0.6
T90 (°C) at 84 kPa	155.3 ± 1.3	160.49 ± 3.87	158.5 ± 11.9	144.95 ± 5.95	159.59 ± 8.53	172.41 ± 6.03	157.67 ± 3.79
Driveability Index (°C) at 1atm *	602.87	601.64	602.50	n/a	602.02	627.35	n/a
Lower heating value (kJ/g)	45.32 ± 0.28	43.87 ± 0.21	42.82 ± 0.34	40.78 ± 0.14	42.77 ± 1	42.76 ± 0.42	39.03±0.28
Density @ 20 °C (g/cm^3)	0.74 ± 0.002	0.75 ± 0.001	0.75 ± 0.001	0.75 ± 0.001	0.75 ± 0.002	0.76 ± 0.003	0.78 ± 0.002
Dynamic viscosity@ 20 °C (cP)	0.36 ± 0.032	0.42 ±0.001	0.43 ± 0.008	0.56 ± 0.009	0.42 ± 0.012	0.49 ± 0.023	0.79 ± 0.015
Kinematic viscosity @ 20 °C (mm^2/s)	0.49 ± 0.042	0.57 ± 0.002	0.57 ± 0.009	0.74 ± 0.011	0.57 ± 0.015	0.65 ± 0.028	1.01 ± 0.017
Copper strip corrosion test, 3 h at 50 °C	1a	1a	1a	1a	1a	1a	1a
Haze point (°C)	n/a	n/a	n/a	n/a	−5 ± 0.47	−11 ± 0.47	−26 ± 1.25
Phase separation (°C)	n/a	n/a	n/a	n/a	−7 ± 0.82	−15 ± 0.82	−28 ± 1.41

* Obtained from the temperatures in Table 4.3

4.3.1 Volatility

The vaporization of a fuel precedes all combustion and can limit the ability and/or rate of the fuel to mix with the air to create the desired homogeneous or stratified charge important for combustion phasing and emissions [23]. As such, the volatility and properties associated with the phase change of the fuel, including vapor pressure, distillation curve, HoV, and the derived vapor lock indices and drivability indices are important properties that must match specification for effective engine operation. There is no single best volatility defined for a smooth drivability because volatility is highly dependent on altitude and seasonal temperature of the location. Three indices are used in the United States to characterize the volatility of a fuel: vapor pressure, distillation curve, and vapor lock index. ASTM D4814 sets limits for vapor pressure, distillation temperatures (at 10, 50, and 90% evaporated points), and vapor lock index. The experimental results for these properties are presented and compared to the gasoline specification ASTM D4814 in Table (Table 4.2).

Vapor pressure: Regarding cold-start and warm-up drivability, vapor pressure is one of the most important fuel properties. Low vapor pressure results in cold start problems while high

vapor pressure can lead to vapor lock and evaporative emissions [76]. The Reid vapor pressure (RVP) is the metric commonly used to characterize a fuel's vaporization potential. The RVP is the vapor pressure (two-phase) at a temperature of 100°F (37.8 °C) while maintaining a volume ratio of the vapor to liquid phase of the sample at 4:1, according to ASTM D 5191 [65]. Generally, mixtures of non-polar hydrocarbons with polar compounds deviate from ideal solution behavior due to formed positive azeotropes. Ethanol can form positive azeotropes with C5-C8 hydrocarbons (alkanes, olefins, aromatics) with normal boiling points in the range from ~30 °C - 120 °C [77].This behavior, stemming from the polarity of ethanol, increases the RVP of the fuel when ethanol is blended with gasoline up to about 45 vol. % [12] despite the much lower RVP of ethanol in its pure state.

The RVP results are presented in Figure 4.1 and Table 4.1. The addition of anhydrous and hydrous ethanol to the base gasoline increased the RVP for the blending ratios selected here. For each blend ratio, the RVP of the hydrous ethanol were higher than the anhydrous ethanol blends, which can be attributed to the higher polarity of water compared to ethanol and the increased potential to form positive azeotropes. For anhydrous blends, the highest RVP was observed for E10 while for hydrous ethanol blends, the highest was H15.

The optimum volatility for fuels highly depends on temperature and altitude of the location. Fuels with moderate volatility are desired for hot seasons and locations with high altitudes while relatively high volatile fuels are required for cold seasons and low altitude regions. To address the dependency of the volatility on elevation and seasonal climatic changes, ASTM D4814 provides six vapor pressure/distillation classes (AA, A, B, C, D, E) and six vapor lock protection classes (1-6) for fuels (Table 4.2). The seasonal and geographic distribution of the combined vapor pressure/distillation-vapor lock classes is specified by an alphanumeric designation that uses a

letter from vapor pressure/distillation classes and a number from vapor lock protection classes. Class AA in vapor pressure/distillation classes accounts for hottest regions while Class E accounts for coldest regions. The maximum allowable RVP for each class is available in the ASTM D4814. Here, E0 was found to qualify for ASTM D4814 Class AA, while all of the blends qualify for Class A.

Table 4.2 ASTM D4814 requirements for Vapor Pressure/Distillation and Vapor Lock Protection classes [11]

	Vapor Pressure/Distillation Class					
	AA	**A**	**B**	**C**	**D**	**E**
Reid vapor pressure (kPa), max	54	62	69	79	93	103
Distillation Temperatures(°C)						
T10, max	70	70	65	60	55	50
T50, min	77	77	77	77	77	77
T50, max	121	121	118	116	113	110
T90, max	190	190	190	185	185	185
End point, max	225	225	225	225	225	225
Driveability Index (°C), max	597	597	591	586	580	569
	Vapor Lock Protection Class					
	1	**2**	**3**	**4**	**5**	**6**
$T_{v/l=20}$ (°C), min	54	50	47	42	39	35

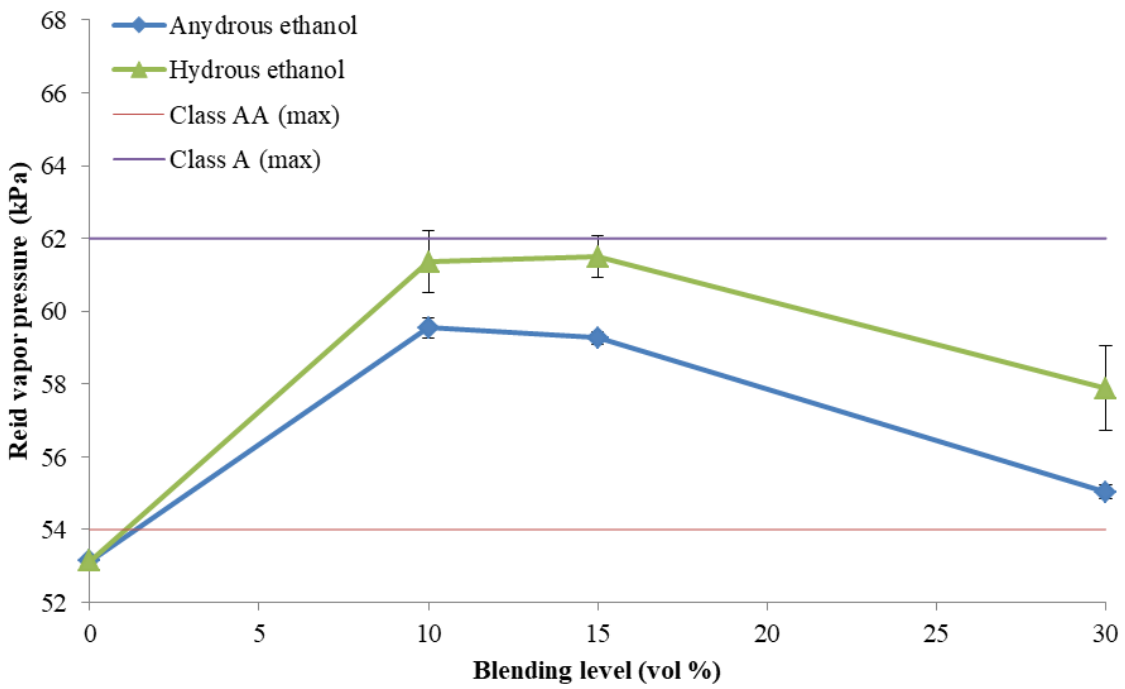

Figure 4.1 Effect of ethanol (anhydrous and hydrous) blending on vapor pressure of gasoline. Error bars represent one standard deviation.

Vapor lock index: The vapor-locking tendency of a fuel can be attributed to its vapor pressure and front end of distillation curve, but the property that best predicts hot fuel handling problems is known as vapor lock index. The vapor lock index is the temperature at which a fuel forms a volumetric vapor-liquid ratio of 20 (V/L = 20) and is shown here with $T_{V/L=20}$. As mentioned in the previous section, the ASTM D4814 identified six vapor lock protection classes (1 to 6) for minimum $T_{V/L=20}$ to eliminate the vapor lock problem. In this classification, Class 1 accounts for hottest regions while Class 6 accounts for coldest regions. A fuel with a higher $T_{V/L=20}$ exhibits greater protection against vapor lock. In this study, vapor lock index was measured according to ASTM D5188 [66] and results are presented in Figure 4.2 and Table 4.1. Results indicated that blending both hydrous and anhydrous ethanol decrease the $T_{V/L=20}$ compared to the baseline gasoline due to the formation of positive azeotropes. This reduction is more intense in the

case of hydrous ethanol because of higher polarity of the water. Thus, at each blend ratio, the $T_{V/L=20}$ of the hydrous ethanol blend was less than that of the anhydrous ethanol blend, which is consistent with results obtained for RVP. All these blends can be best categorized under ASTM D4814 Class 1 (minimum of 54 °C).

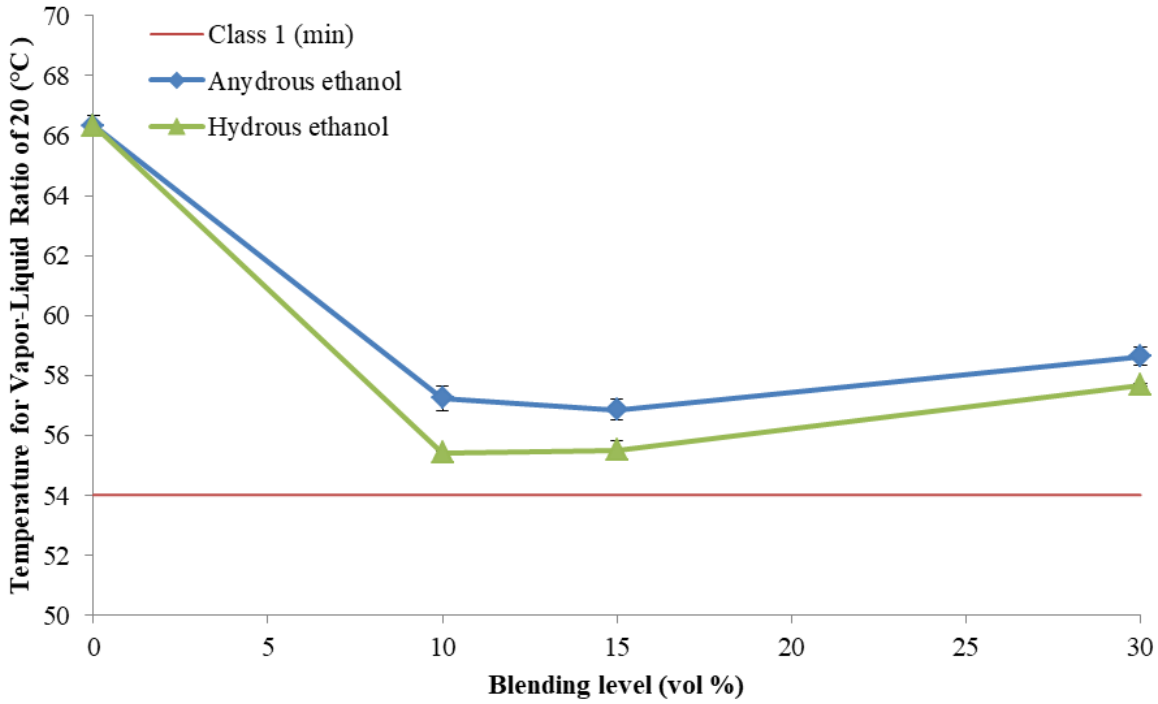

Figure 4.2 Effect of ethanol (anhydrous and hydrous) blending on vapor lock index of gasoline. Error bars represent one standard deviation.

Distillation curve: A distillation curve is a plot of the boiling temperature of a fluid mixture versus the volume fraction distilled and can be related to parameters such as engine startability, icing and vapor lock in the fuel system, fuel autoignition, fuel injection schedule, and even exhaust emissions in both gasoline and diesel engines [78-80]. Conventionally, gasolines are composed of compounds with boiling points ranging from about 20 to 225 °C [81]. Front-end volatility (T0 to T20) has a vital role in cold start, engine warm-up, evaporative emissions, and vapor lock. Midrange volatility (T20 to T90) is relevant to fuel economy [59], warming up,

acceleration, and cold weather performance [81]. The tail-end volatility (T90 to end-point) which represents the fraction of hydrocarbons with high boiling points is important to avoid the formation of deposits inside the engine and particulate matter formation [82]. Usually SI engines are relatively flexible and are not highly affected by small changes in the distillation curve. The ASTM D4814 sets maximum boundaries for T10, T90, and end point distillation temperatures and a boundary range for T50. T10 should be lower than maximum allowable limits to provide a fast start of the engine at cold temperatures and low engine RPM. T50 is adjusted to ensure the balance between low and high boiling point compounds. End-point is set to a maximum of 225 °C as components with higher boiling temperatures can cause combustion failure due to reduced fuel/air mixing as well as oil dilution [81].

In this study, an advanced distillation apparatus was used to obtain distillation curves at ambient pressure of 84 kPa for gasoline, gasoline-hydrous ethanol and gasoline-anhydrous ethanol blends. Distillation curves are depicted in Figure 4.3. Distillation temperatures (initial boiling point, T10, T50, T90) for each of the blends are listed in Table 4.1. No evident difference was observed among initial boiling points of blends and gasoline; however, it was observed that ethanol (anhydrous and hydrous) addition significantly changes the shape of the distillation curve. These changes can be attributed to the near-azeotropic behavior of ethanol-gasoline blends as discussed earlier. The near-azeotropic behavior is apparent from a localized near-flat region in the distillation curve and is more accentuated when large amounts of oxygenate is used as observed for E30 and H30 in Figure 4.3 [83]. All ethanol blends (hydrous and anhydrous) reduced the front end and midrange distillation temperatures notably due to the formation of azeotropes. Lower boiling temperatures are noticed compared to the unblended gasoline for the first 50% evaporated for the 10 and 15% ethanol mixtures and nearly 75% of the distillation curve for the 30% mixtures. The

tail-end volatilities for all blends are approaching to that of gasoline so that changes in T90 compared to the base-gasoline are negligible as most of the ethanol and water are evaporated by this point. Small differences between blends at the tail-end can be attributed to the reduced concentration of heavy hydrocarbons due to dilution and through the formation of azeotropes with the ethanol and water resulting in their accelerated elution from the liquid phase. For ethanol blends, the sudden rise in boiling temperatures after the nearly isothermal boiling behavior occurs at volume fractions corresponding to the point at which all the ethanol is evaporated, resulting in the convergence of the distillation curves to that of the E0 fuel.

At each blend ratio, hydrous and anhydrous ethanol blends presented similar patterns and their differences are statistically negligible. All hydrous ethanol blends demonstrated slightly faster temperature rise at the inflection point where the distillation curve approaches to that of the E0 possibly explained by increased positive azeotropic behavior of water.

In this study, distillation temperatures were also compared to the ASTM D4814 limits at atmospheric pressure to investigate the compatibility of these blends with the current standards. Since distillation temperatures were obtained at 84 kPa, temperature readings were corrected to 101.3 kPa pressure by applying the correction by means of the Sydney-Young equation (eq. 1) as stated in ASTM D86 [84]:

$$C_c = 0.0009\ (101.3 - P_k)(273 + t_c) \qquad \text{Eq.4.1}$$

Where C_c is the correction factor added algebraically to the observed temperature readings, P_k is barometric pressure at the time and location of the test (84 kPa), and t_c is the observed temperature reading in °C. The corrected temperatures are tabulated in Table4.3. Based on ASTM criteria, only the gasoline exceeded T10 test requirements while all the other fuel blends were within the temperature limits for at least one of the volatility classes.

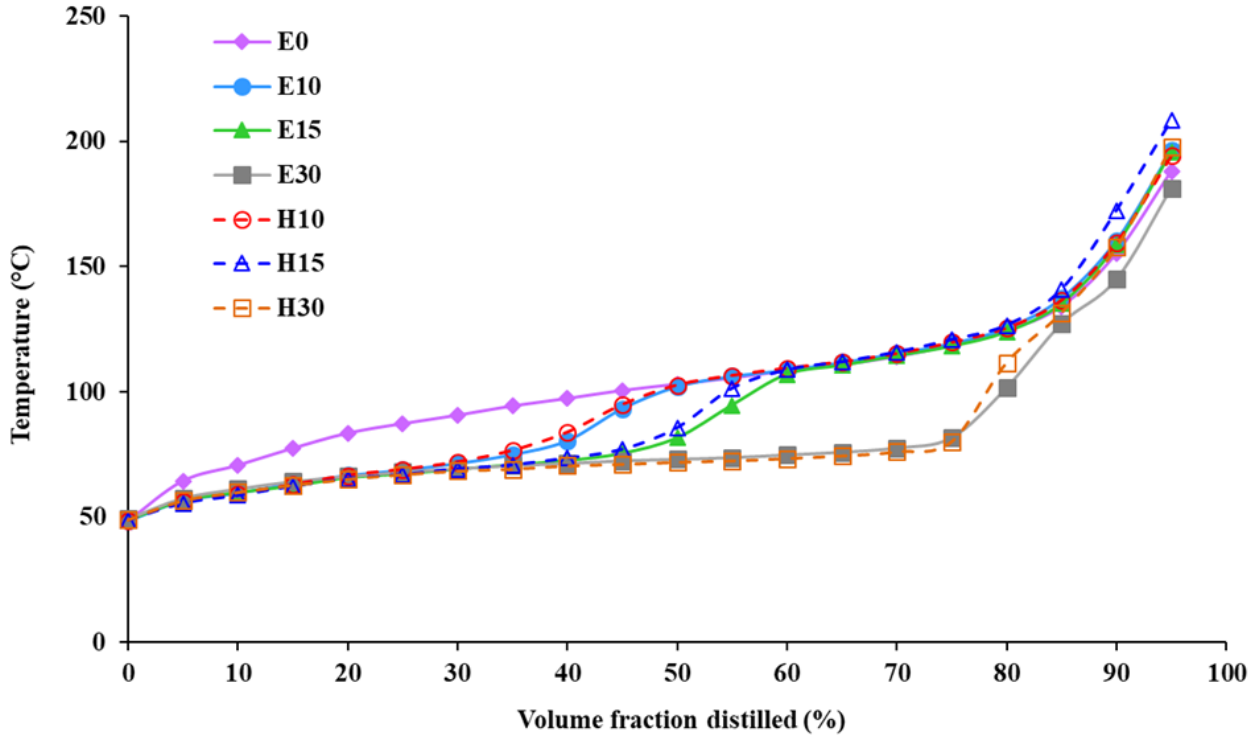

Figure 4.3 Distillation curves for gasoline and blends of hydrous and anhydrous ethanol at 84 kPa. Data represent the average of two distillation tests with average coefficient of variation of 1.69%.

Table 4.3 Corrected temperatures for 1 atm

	Gasoline (E0)	E10	E15	E30	H10	H15	H30
Initial boiling point (°C) at 1 atm	53.40	53.45	53.61	54.32	53.63	53.67	53.86
T10 (°C) at 1 atm	76.06	64.78	64.85	66.46	64.45	63.75	65.07
T50 (°C) at 1 atm	108.94	107.97	87.03	78.54	108.57	91.16	77.30
T90 (°C) at 1 atm	161.97	167.24	165.22	151.46	166.33	179.34	164.38

Drivability index: Drivability index is another parameter in the ASTM D4814 which is a function of T10, T50 and T90 in order to consider distillation parameters and ethanol content influences on controlling cold start and warm-up drivability. The values for drivability indices are available in Table 4.1 for distillation temperatures tabulated in Table 4.3. For E10 and H10, the equation provided in the standard for gasoline and gasoline-ethanol blends containing up to 10% by volume ethanol was used:

$$DI_c = 1.5\,T_{10} + 3\,T_{50} + T_{90} + 1.33 \times (Ethanol\ \%\ by\ volume) \quad \text{Eq.4.2}$$

For E15 and H15 the equation describing gasoline-ethanol blends containing greater than 10% by volume and no more than 15% by volume ethanol was used:

$$DI_c = 1.5\,T_{10} + 3\,T_{50} + T_{90} + 5.26 \times (Ethanol\ \%\ by\ volume) \quad \text{Eq.4.3}$$

It is not clear how the equation would be modified for the application of blends containing more than 15% by volume ethanol; therefore, this parameter was not applicable to E30 and H30. Results showed that all blends exceeded the maximum limits and were qualified for none of the classes possibly because the T10 for the base gasoline is out of the acceptable range. Use of gasoline with better front-end volatility characteristics may eliminate this drawback.

Distillate Composition: The evolution of the composition of unblended gasoline and the oxygenated blends during the distillation was measured by sampling and analyzing the condensate (distillate) samples during the distillation process. The distillate ethanol, H_2O, and aromatic concentrations are shown in Figure 4.4. From the sharp rise in the concentration of aromatics once the ethanol and water (if present) were nearly completely evaporated, it can be inferred that the presence of ethanol and water suppressed the distillation of aromatic species. The larger initial concentration of oxygenates results in a longer delay prior to the evaporation of the aromatics, causing an enrichment in the liquid fuel in the aromatics at late stages of the distillation. Interestingly, the mass percentages of aromatics are relatively close for all blends at the end of the distillation (in the range of 71–79% at 90% distilled) despite having very different initial amounts depending on the initial oxygenate concentration. These observations, coupled with the fact that aromatics have shorter kinetic pathways to produce soot [85], may partially explain recent observations of increased PM emission when using blends containing moderate ethanol concentrations (20-40 vol%) in DISI engines [86, 87]. Figure 4.4 also shows that the differences

between hydrous and anhydrous blends in the suppression of aromatic compounds are negligible. Interestingly, however, at the beginning of each distillation, while water is being evaporated, the concentration of ethanol in the anhydrous ethanol blends is 14.8% higher in average than in the corresponding hydrous ethanol blends possibly due to the formation of ternary azeotropes (ethanol/water/non-polar hydrocarbons) in the case of the hydrous ethanol blends.

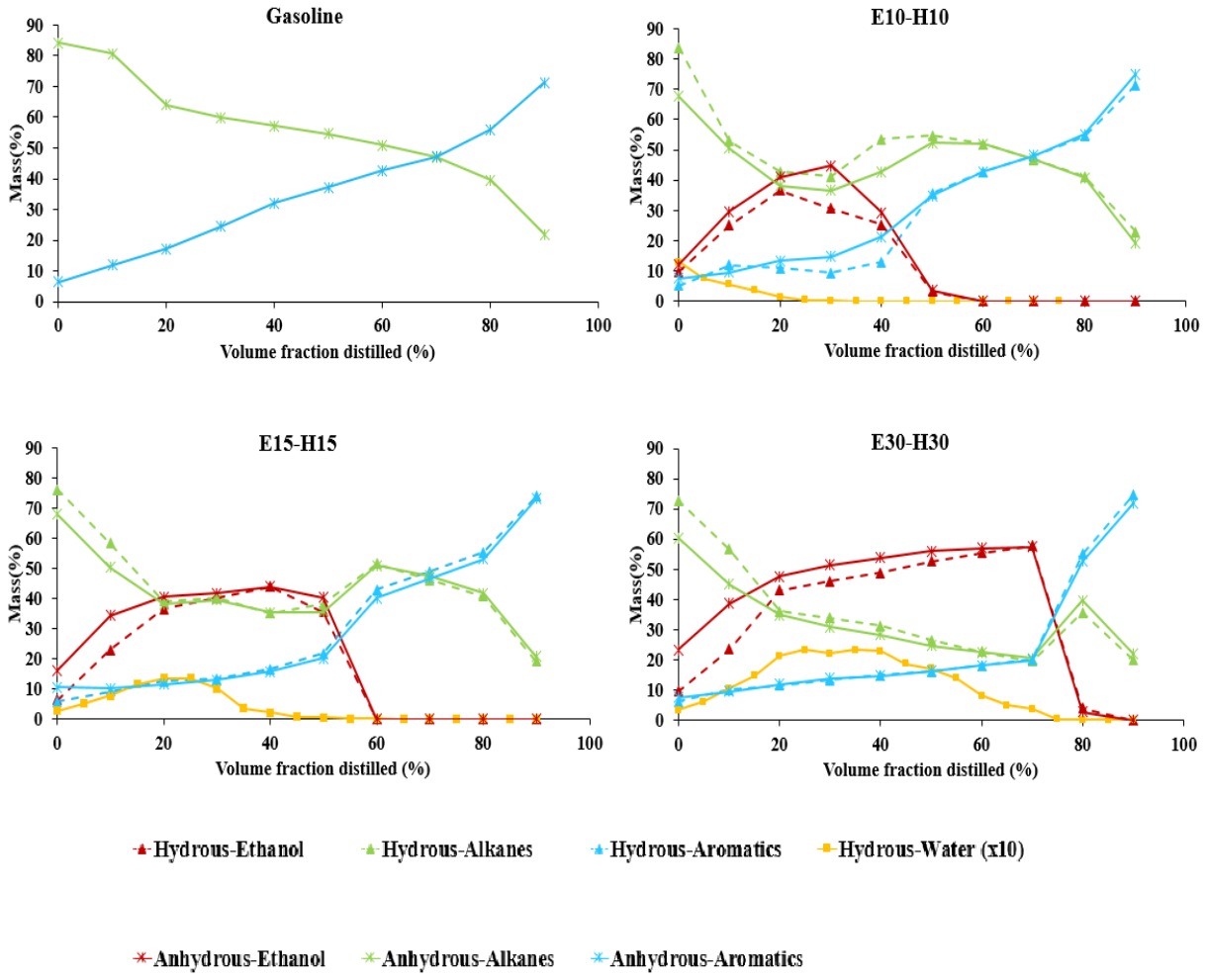

Figure 4.4 Results of the detailed distillate composition analysis for gasoline and blends of hydrous (dotted lines) and anhydrous (solid lines) ethanol in gasoline. E: anhydrous ethanol blends. H: hydrous ethanol blends. The average coefficient of variations of the data was calculated to be ±4.06%.

Distillation model validation: The distillation model used in this study which is developed by Backhaus [73] uses UNIFAC theory to predict non-ideal VLE of the oxygenate-hydrocarbon mixtures, distillation curves, and compositions. The initial compositions of the blends were used as inputs for the simulations. There was a strong agreement between the predicted and measured distillation curves for gasoline, anhydrous, and hydrous blends (Figure 4.5) as well as agreement between the measured and predicted molecular weight of the distillate for the same fuels (Figure 4.6). These results demonstrate that the model is accurate and capable of predicting the physics required to characterize the vaporization behavior of the anhydrous and hydrous blends. Thus, the results of the droplet model [74] which is derived from the distillation model can be used with confidence.

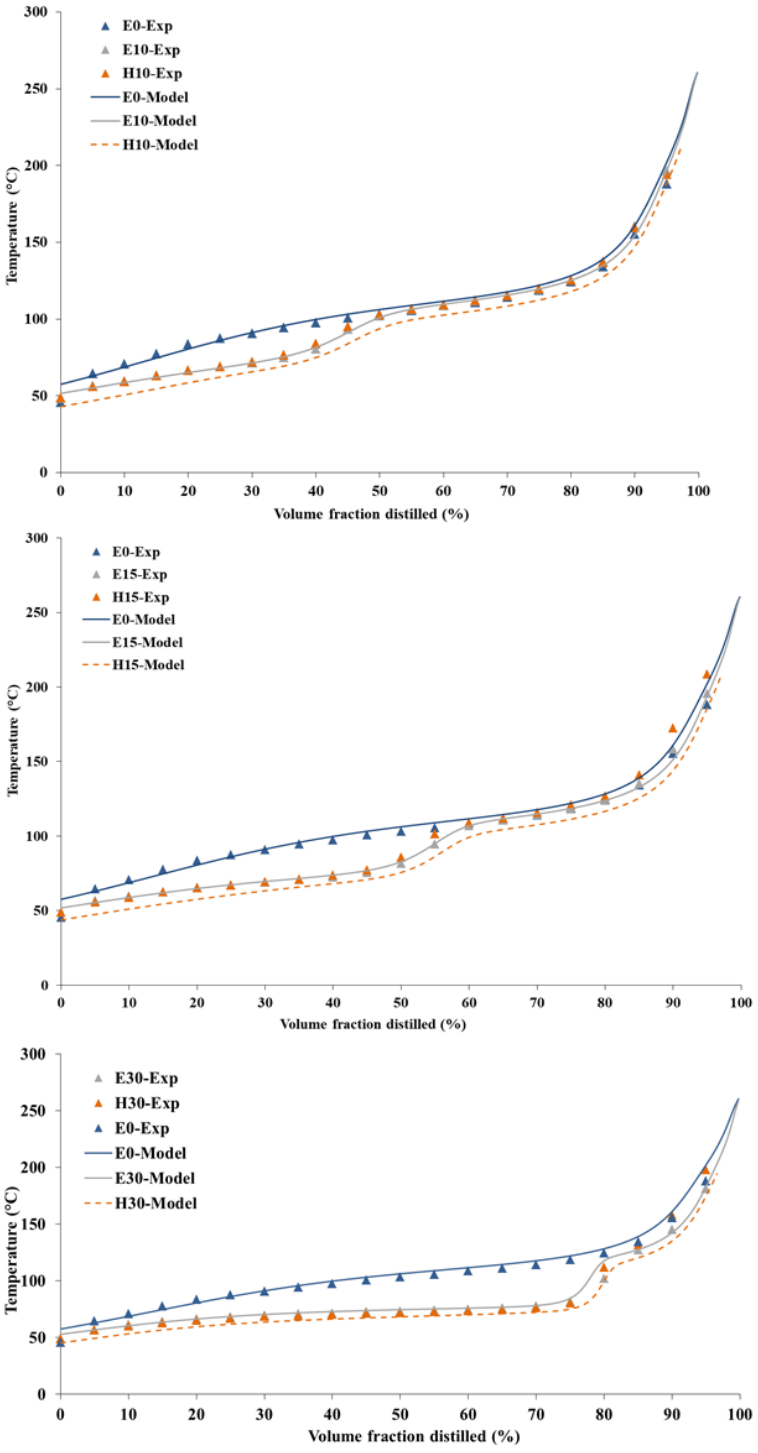

Figure 4.5 Comparison of experimental distillation curves to those modeled. Exp: Experimental distillation curves. Model: predicted distillation curves. E: anhydrous ethanol blends. H: hydrous ethanol blends.

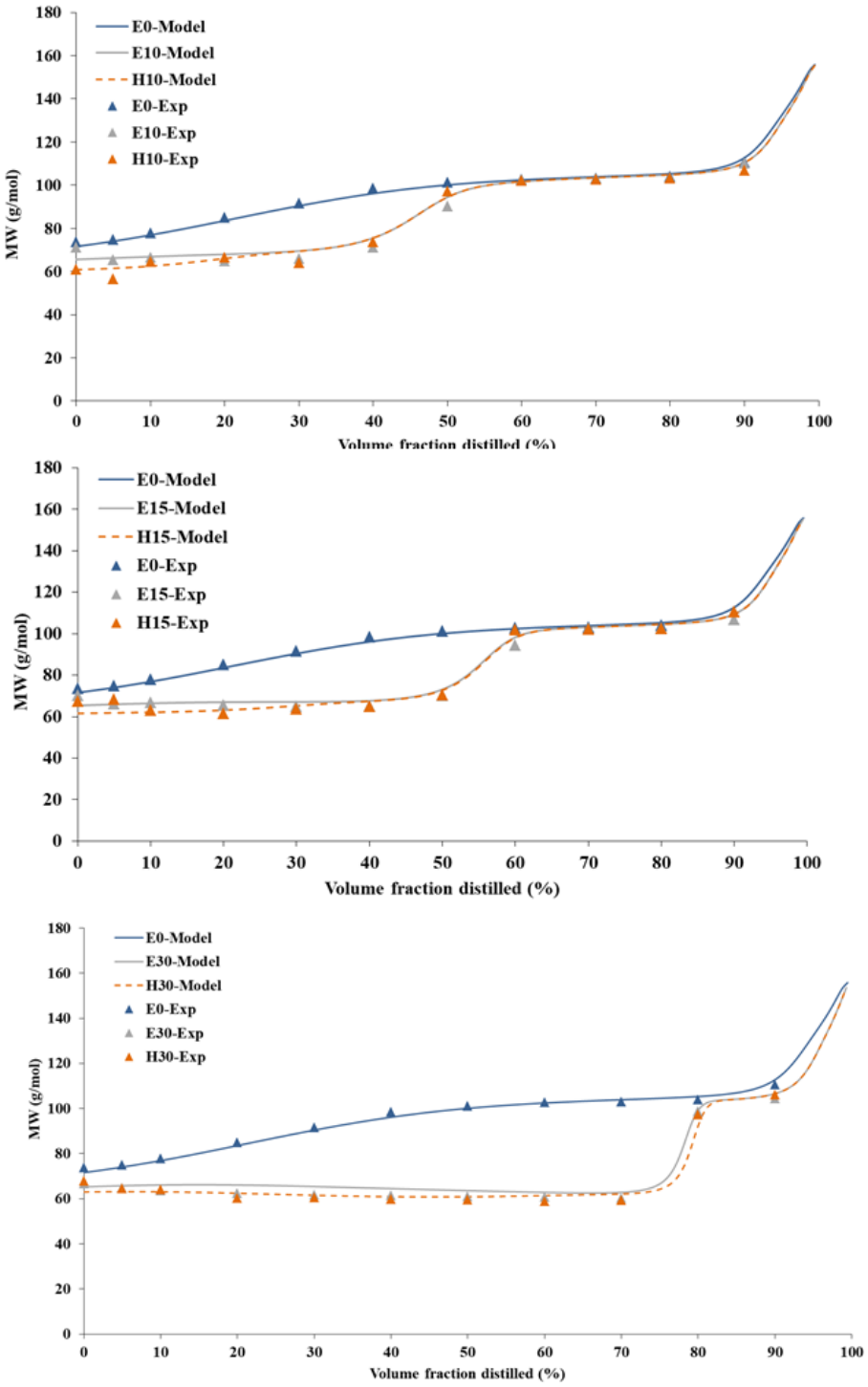

Figure 4.6 Comparison of experimentally measured and predicted average molecular weight. Exp: Experimental average molecular weight. Model: predicted average molecular weight. E: anhydrous ethanol blends. H: hydrous ethanol blends.

Droplet lifetime: The droplet evaporation model can track evaporation rate, composition, and HoV of a single droplet as it responds to temperature changes due to heat conduction and evaporative cooling. In this study, this model was used to monitor how higher heat of vaporization and heat capacity of water relative to ethanol and iso-octane, as a representative hydrocarbon in gasoline, can change the vapor-liquid equilibrium (Table 4.4). Results of the droplet model were used to link oxygenate content to possible PM emissions stemming from incomplete evaporation. Although there are sooting indices such as the Particulate Matter Index (PMI) [85], they do not incorporate the non-ideal interactions between oxygenates and hydrocarbons in determining a mixture's tendency to soot in a DISI engine. The droplet model is not able to quantify PM emissions, but Burke et al. [74] showed that the measured PM correlated better with the predicted liquid mass of aromatic remaining in an oxygenate blend at gasoline's net evaporation time than with the PMI.

Table 4.4 latent heat of vaporization and heat capacities of water, ethanol, and iso-octane at 298 K [88].

Property	Water	Ethanol	Iso-octane
Latent heat of vaporizations (kJ/kg)	2441.38	923.90	347.01
Heat capacity (J/kg.K)	4185.50	2460	2201.08

As a reference state, all blends were modeled as 25-μm droplets in a constant ambient temperature (323 K) at atmospheric pressure. An injector's nozzle design, operational conditions, and the physical properties of the fuel can influence the spray characteristics including droplet sizes. A diameter of 25 μm was chosen because this is in the usual range for mean droplet diameters produced with traditional DISI injector technology [89]. The data in 4.11 and Figure 4.12 show that oxygenates (ethanol and water) increase the HoV of the mixture, resulting in a greater initial temperature drop. This trend is more observable in blends with higher blending ratios of

oxygenates. The hydrous ethanol mixtures exhibit a noticeable difference in the transient HoV when compared to the anhydrous counterpart (Figure 4.7), resulting from the high HoV of water. However, this does not translate into a noticeable difference in the droplet temperature between the hydrous and anhydrous mixtures (Figure 4.8). The similarities in droplet temperature despite differences in HoV may be due to the low concentration of water in these blends and from the relatively high specific heat capacity of water, which suppresses the temperature change. Furthermore, as the temperature difference between the ambient environment (323 K) and the droplet increase, conductive heat transfer becomes more dominant in heating the droplet than the evaporative cooling. The HoV and temperature remain high and low, respectively, until ethanol and water are evaporated as shown in Figure 4.9. After depletion of oxygenates, temperature and HoV of all droplets converge with that of gasoline.

Although the addition of oxygenates depresses the droplet temperature and increases the HoV at early stages of evaporation, the model predicts that complete evaporation of the base gasoline (E0) droplet takes longer than all of the other blends (Figure 4.11). These results are opposite to results of Burke et al. [74], in which blends containing ethanol (regardless of concentration) had longer evaporation times relative to the base gasoline at temperatures higher than 315 K when a droplet diameter of 50 μm was used. This discrepancy can be attributed to the difference in the type of the gasoline used as well as the droplet size. The gasoline used in the study of Burke et al. [74] was FACE B, which is a lighter fuel with a relatively high volatility and low concentrations of heavy hydrocarbons. In contrast, the UTG 96 gasoline used in our experiments contains a higher fraction of heavy hydrocarbons and exhibits a much larger T50 than the FACE B fuel. The shorter droplet evaporation time experienced for the oxygenated fuels, despite having higher HoV relative to gasoline, implies that volatility is the dominant factor for

the given temperature, fuel, and droplet size examined here. The difference in volatility between the oxygenated and non-oxygenated blends is clear from the distillation curves (Figure 4.3) and the transient droplet vapor pressure profiles (Figure 4.10). Moreover, no significant difference in the droplet evaporation time was observed between anhydrous and hydrous ethanol blends with the same blending ratios, an expected result given the similarities in overall volatility and droplet temperature (Figures 4.3 and 4.12).

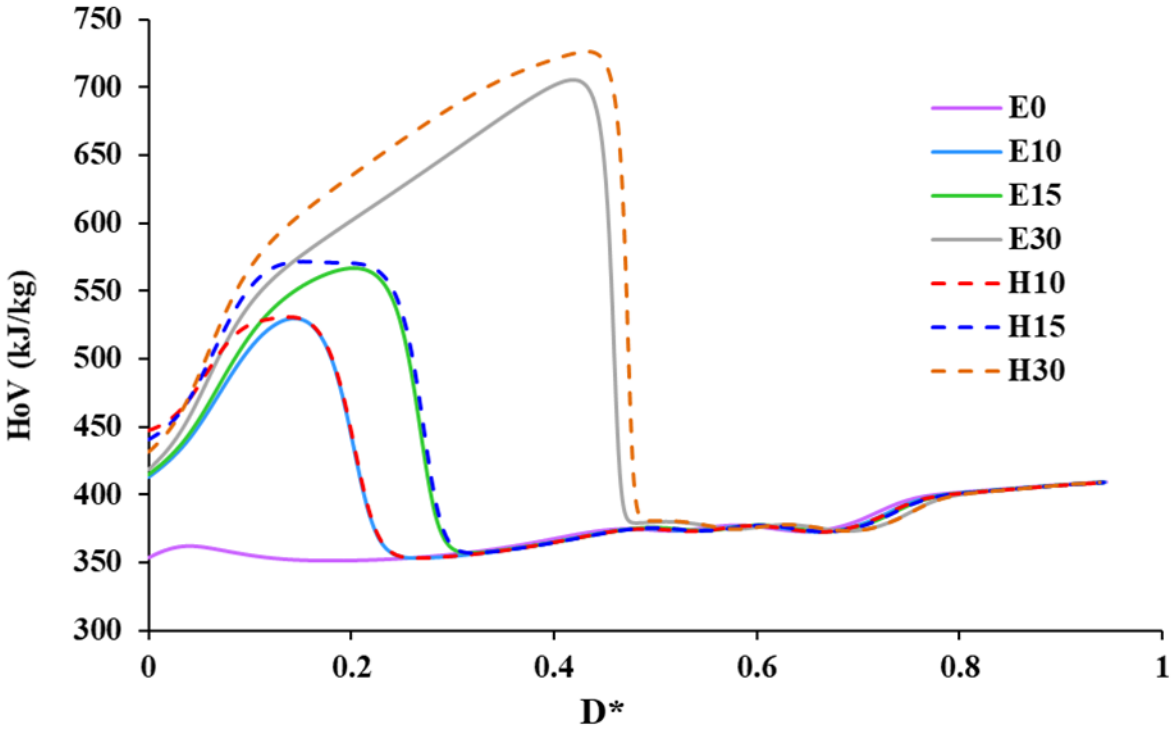

Figure 4.7 HoV profiles of each blend obtained from the droplet evaporation model as a function of dimensionless D* at 1 atm and 323 K. (initial droplet diameter (D0) = 25 µm). E: anhydrous ethanol blends. H: hydrous ethanol blends. D: Diameter. D0: Initial diameter. D*=1-D/D0.

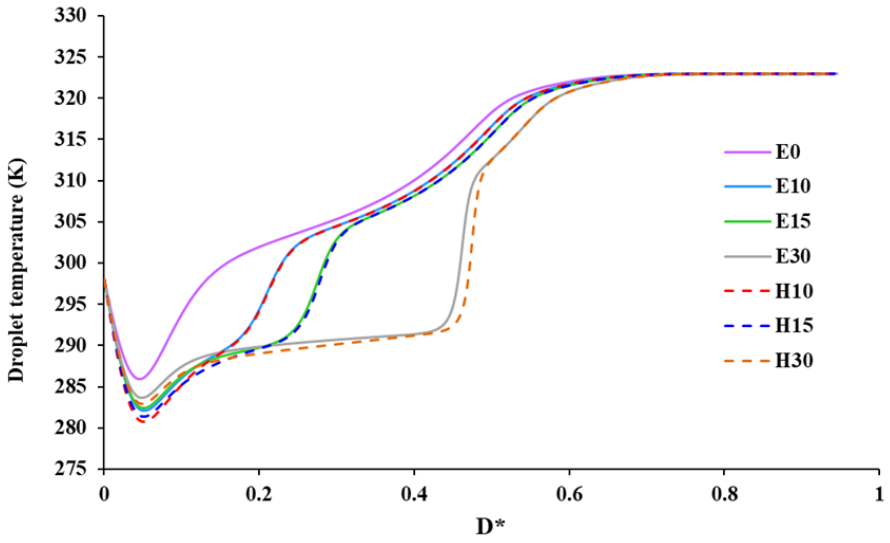

Figure 4.8 Temperature profiles of gasoline and blend obtained from the droplet evaporation model as a function of dimensionless D* at 1 atm and 323 K. (D0= 25 µm). D*=1-D/D0. E: anhydrous ethanol blends. H: hydrous ethanol blends.

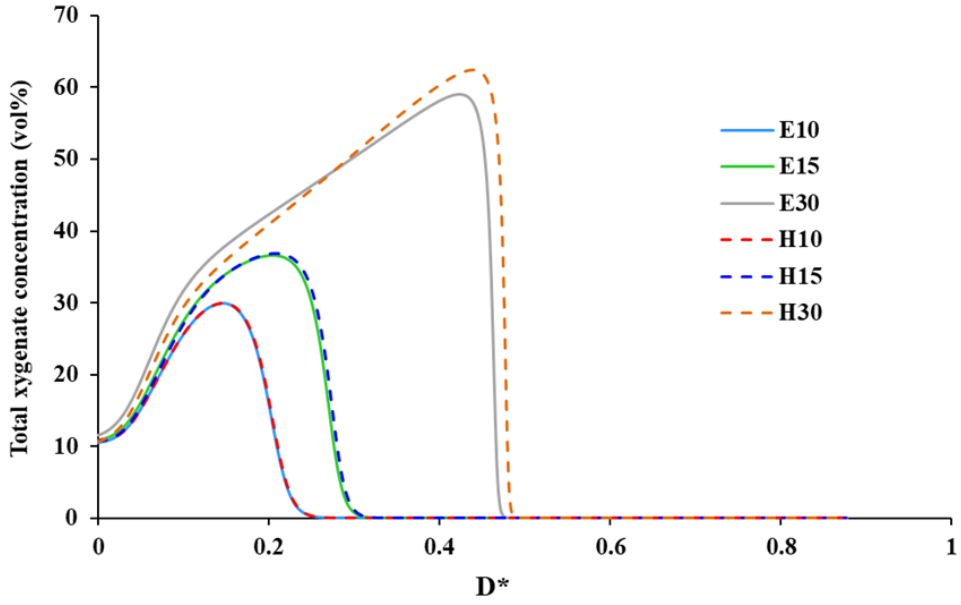

Figure 4.9 Total concentration of ethanol/water profiles of gasoline and blend obtained from the droplet evaporation model as a function of dimensionless D* at 1 atm and 323 K. (D0= 25 µm). D*=1-D/D0. E: anhydrous ethanol blends. H: hydrous ethanol blends.

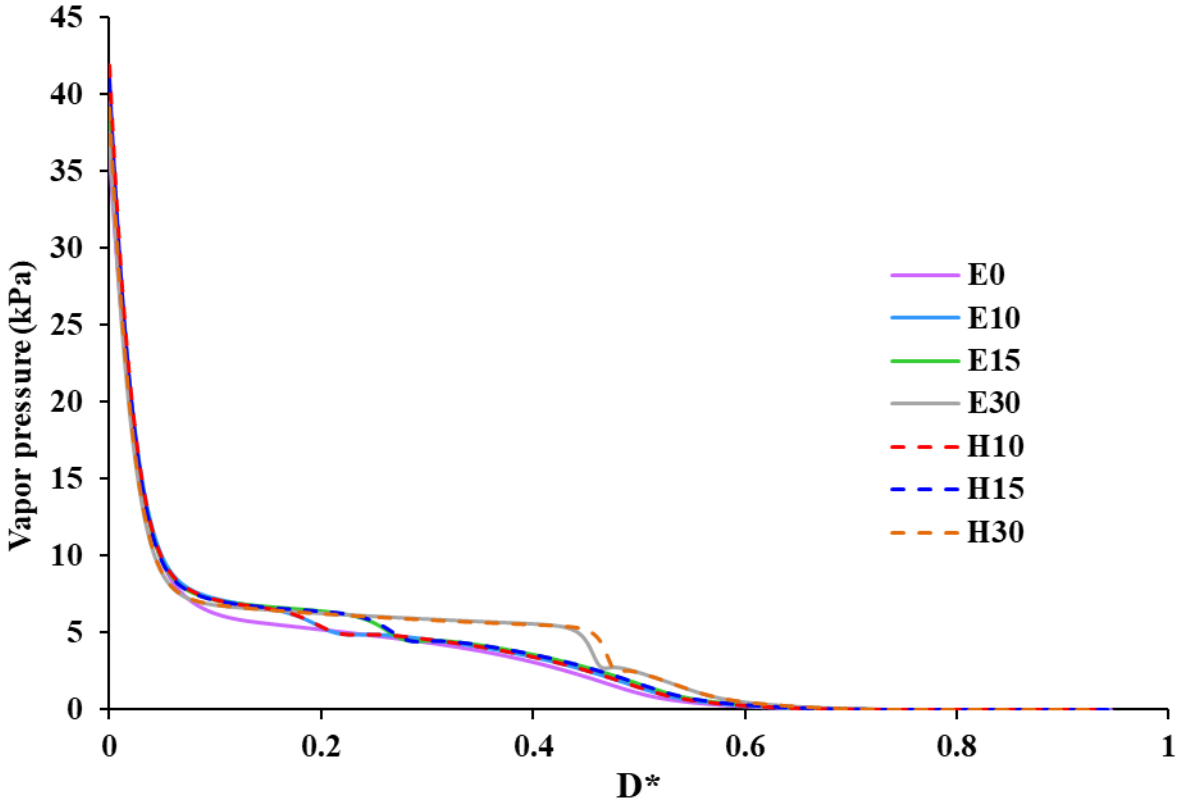

Figure 4.10 Vapor pressure profiles of each blend obtained from the droplet evaporation model as a function of dimensionless D* at 1 atm and 323 K. (initial droplet diameter (D0= 25 µm). E: anhydrous ethanol blends. H: hydrous ethanol blends. D: Diameter. D0: Initial diameter. D*=1-D/D0.

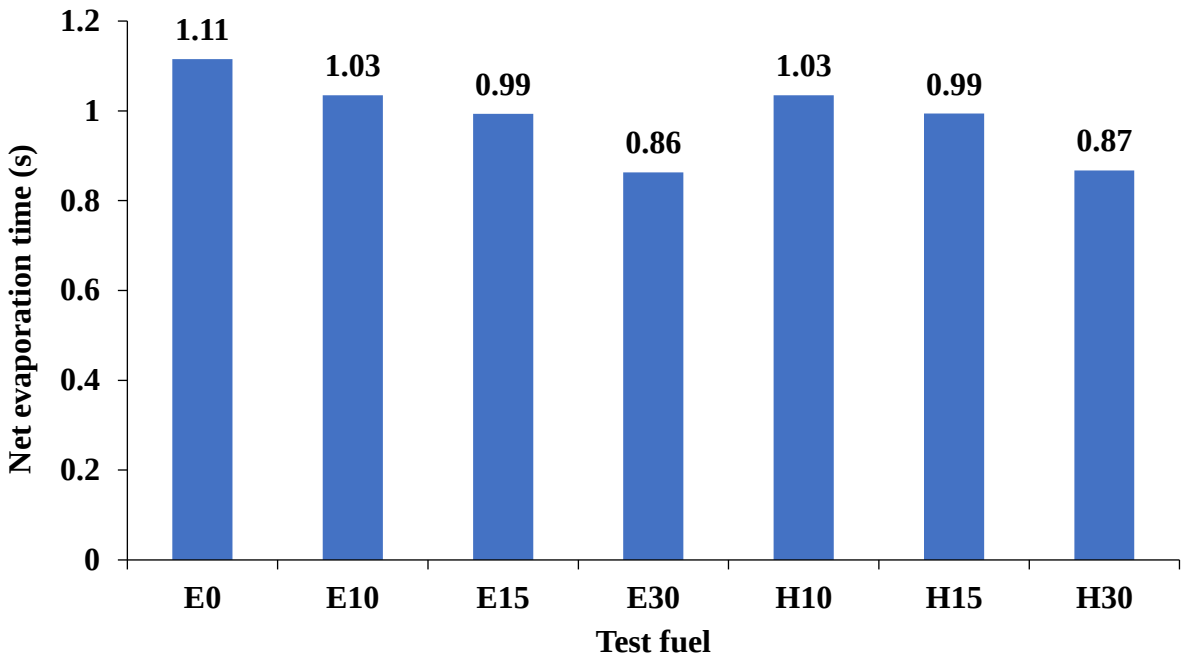

Figure 4.11 Droplet evaporation time for all blends obtained from droplet evaporation model for a constant ambient pressure and temperature of 1 atm and 323 K, respectively (droplet diameter= 25 µm).

Modified droplet lifetimes based on measured and predicted physical properties: The physical properties (especially viscosity, density and surface tension) of a fuel are important factors in atomization, spray pattern, and mixture formation. The addition of water non-linearly increases the viscosity and density of hydrous ethanol blends compared to anhydrous blends, especially at medium and high blending ratios. This can be problematic because larger droplets in the cylinder caused by poor fuel atomization can increase spray tip penetration resulting in a reduced spray angle, slower evaporation, and increased susceptibility for incomplete mixing and pool generation/burning, all of which increase chances of PM/soot exhaust emissions [43]. To take these physical properties into account, a model developed by Elkotb [90, 91] was exploited to

estimate the initial droplet size of all the fuel blends (or the relative proportion to that of gasoline) based on bulk fluid physical properties:

$$\text{Sauter Mean Diameter} = 3.085 \nu_l^{0.385} \sigma_l^{0.737} \rho_l^{0.737} \rho_g^{0.06} \Delta P_l^{-0.54} \quad \text{Eq.4.4}$$

In Eq. 4, ν_l is the viscosity of liquid, ρ_g and ρ_l are the gas and liquid density, σ_l is the surface tension of liquid and ΔP_l *is* the difference between injection pressure and ambient pressure. Since ΔP_l is identical for all blends, the initial droplet diameter of gasoline was assumed to be 25 μm and the droplet sizes of the other blends relative to that of E0 were determined using Eqn. 4 with the physical properties listed in Table 4.5. Density and kinematic viscosity are obtained experimentally while surface tension was calculated by using DIPPR 801 Database [92]. To determine the influence of droplet size on droplet evaporation lifetime, the droplet evaporation model was used with the new calculated droplet sizes for each blend at constant ambient temperature (323 K) at 1 atm pressure. In contrast to previous simulations, the results of using the refined estimate of initial droplet size reveal that oxygenated blends result in longer droplet evaporation times than that of the base gasoline (Figure 4.12). This result shows that the higher HoV and viscosity of water relative to ethanol together are effective factors that contribute to notable differences in the net evaporation time between the hydrous and anhydrous blends, especially at 15 and 30 vol% blending ratios. As such, once accounting for changes in properties responsible for droplet atomization, fuels containing hydrous ethanol may possess slower in-cylinder evaporation behaviors and as a result would be potentially more prone to produce PM emissions.

Table 4.5 Physical properties of the test fuels and corresponding droplet sizes obtained from the Elkotb model [90]. [a] *Obtained from [92]*.

Fuel	Kinematic viscosity (mm^2/s)	Surface tension (N/m) [a]	Density (g/cm^3)	Initial droplet size (µm)
Gasoline	0.49	0.02158	0.74	25.00
E10	0.57	0.02158	0.75	26.49
E15	0.58	0.02159	0.75	26.85
E30	0.74	0.02156	0.75	29.40
H10	0.57	0.02178	0.75	26.64
H15	0.65	0.02189	0.76	28.46
H30	1.01	0.02216	0.78	34.42

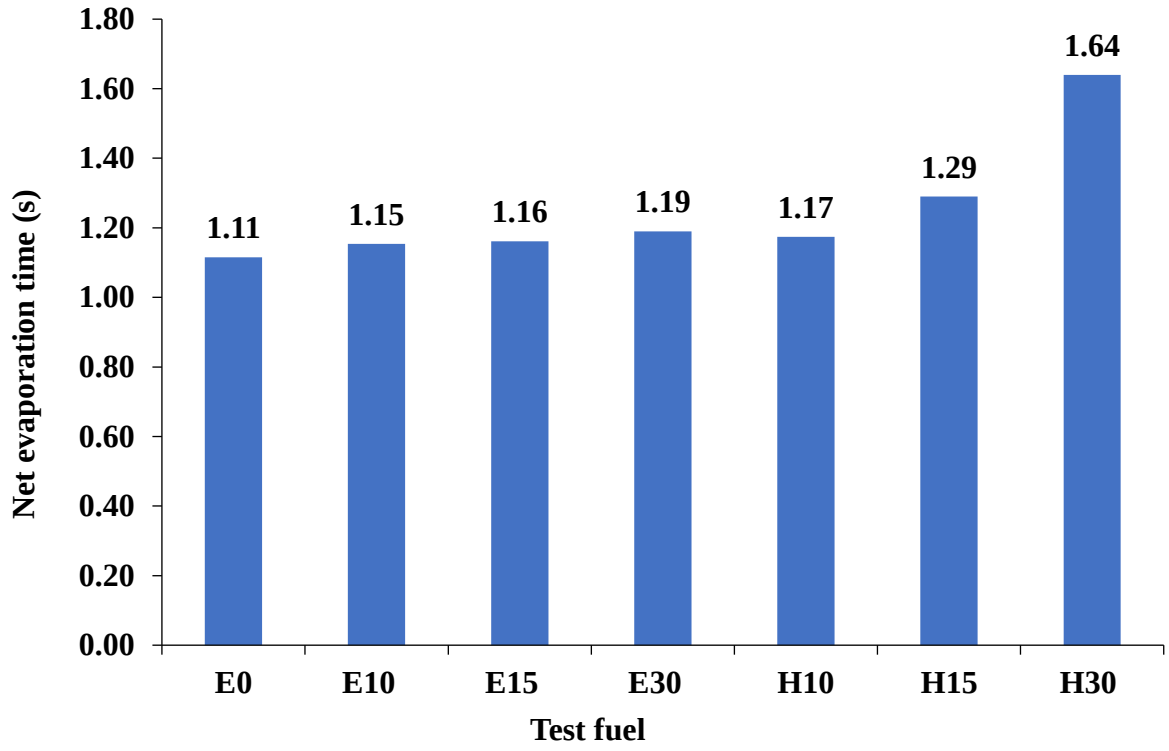

Figure 4.12 Droplet evaporation time for all blends obtained from droplet evaporation model with initial droplet sizes listed in Table 4.5 2 at 323 K and 1 atm.

4.3.2 Corrosion and water phase stability

In this study, copper strip corrosion test was conducted on samples according to ASTM D130-12 [62] to ensure that there would be no corrosion to fuel system metals due to reactive

sulfur compounds in the fuel. However, corrosion is not limited to sulfur corrosion. Generally, ethanol can cause corrosion in three ways: (1) Ethanol is a relatively strong solvent due to the high polarity and can be corrosive to some metallic and non-metallic parts of the engine which is known as dry corrosion [20], (2) Low quality commercial oxygenates may contain ionic impurities such as chloride ions and acetic acid which can be corrosive [20], (3) ethanol is highly hygroscopic and is able to absorb water which can trigger phase separation especially at low temperatures when the amount of water adjacent to the fuel is massive. Consequently, a corrosive mixture of water and ethanol can form at the bottom of fuel tanks which can also adversely affect the combustion by reducing the octane value of the fuel [93]. Stability of water in ethanol-gasoline blends is a function of ethanol concentration, temperature, gasoline composition and presence of co-solvents [77]. As it is shown in Table 4.1, data reported concerning corrosion for all samples was 1a (slight tarnish) which means no corrosion. In addition, no notable difference was observed in the appearance of the copper strips when submerged in the fuels containing different amounts of ethanol and water. Note, the measurements were taken with completely miscible samples, however, based on facts mentioned above, it is essential to identify the phase separation temperatures for hydrous ethanol-gasoline blends.

Phase separation temperatures were determined according to ASTM D 6422–99 [63]. In this method, fuel is cooled at a controlled rate and is checked for phase separation at each temperature. Furthermore, haze point was measured which is the temperature prior to phase separation point when cloudiness in the liquid is observed visually which is then followed by an ice crystal formation (or phase separation). Results showed that phase separation for hydrous ethanol blends with higher ethanol content (and accordingly higher water content) occurred at lower temperatures. The lowest phase separation temperature was observed at -28 $^{\circ}$C for H30

followed by H15 (-15 °C) and H10 (-7 °C). Therefore, separation issues can be mitigated by using high blending ratios, despite the total amount of water in the fuel increasing. This behavior can be attributed to the high hygroscopicity of ethanol so that hydrous ethanol blends with higher blending ratios (i.e. blends with higher ethanol content) are able to keep more water with no phase separation at low temperatures. It was also observed that the separated phase was not in a crystalline form; i.e., water absorbed a portion of the ethanol due to ethanol's hygroscopic nature. Therefore, the mixture is not frozen at such a low temperature (below 0 °C). It can be considered damaging because not only a corrosive mixture of water-ethanol is formed, but also this phenomenon lowers the ethanol concentration in the fuel as the separated ethanol/water mixture may remain in the fuel tank. A fuel with lower content of ethanol relative to the original state has a lower octane value and oxygen content which can adversely impact the combustion and emission characteristics. Relatively high phase separation temperatures especially for the blends containing low and medium hydrous ethanol concentrations indicate that it may be necessary to use additives such as higher alcohols to avoid phase separation.

4.3.3 Lower heating value

Since the heating value of ethanol is lower than that of gasoline, blending ethanol with gasoline will subsequently decreases the heating value of the blend. Thus, to produce the same power output for a given gasoline-fueled engine (at a given compression ratio), more mass of fuel for an ethanol-gasoline blend must be injected in each cycle compared to a non-oxygenated gasoline. This is needed since the air-fuel ratio must be kept as close as possible to stoichiometric ratio in SI engines to fully take advantage of the three-way catalyst. However, since ethanol is more resistant to autoignition, a higher compression ratio can be used to compensate for lower heating value and lower stoichiometric air-fuel ratio. The LHV results are presented in Figure 4.13

and Table 4.1. The addition of water, as expected, reduced the heating value of the hydrous ethanol fuel blends due to its zero calorific value, however, due to the small amounts of water presence in each hydrous ethanol mixture, differences compared to the anhydrous (with same ethanol blending ratios) blends were small (less than 5%) even at 30% by volume.

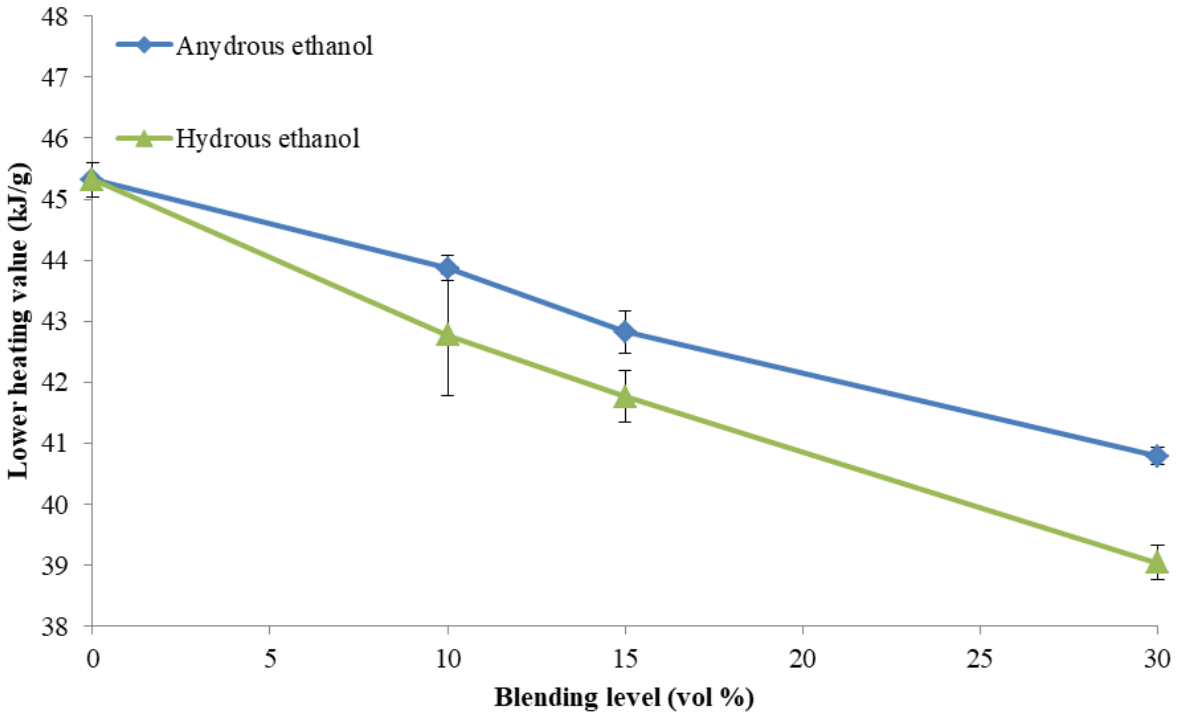

Figure 4.13 Effect of ethanol (anhydrous and hydrous) blending on lower heating value of gasoline. Error bars represent one standard deviation.

4.3.4 Viscosity and density

No limit is specified for density and viscosity in ASTM D4814; however, appropriate values for density and viscosity are vital to enhance the atomization, spray pattern, and mixture formation (as shown in the section 3.4.1.4.2), and consequently reduce the emissions especially in direct injection systems [94]. Results showed that higher density and viscosity of water compared to both ethanol and gasoline non-linearly increased the viscosity and density of hydrous ethanol blends compared to anhydrous ethanol blends especially at higher blend levels (15% and 30%) as

it is shown in Figure 4.14. This may be problematic due to the formation of larger droplet sizes, especially in direct injection systems, as droplet diameters have been shown to increase proportionally with the kinematic viscosity [91]. At the same time, however, increased viscosity may provide better lubrication and less wear in engine parts [20].

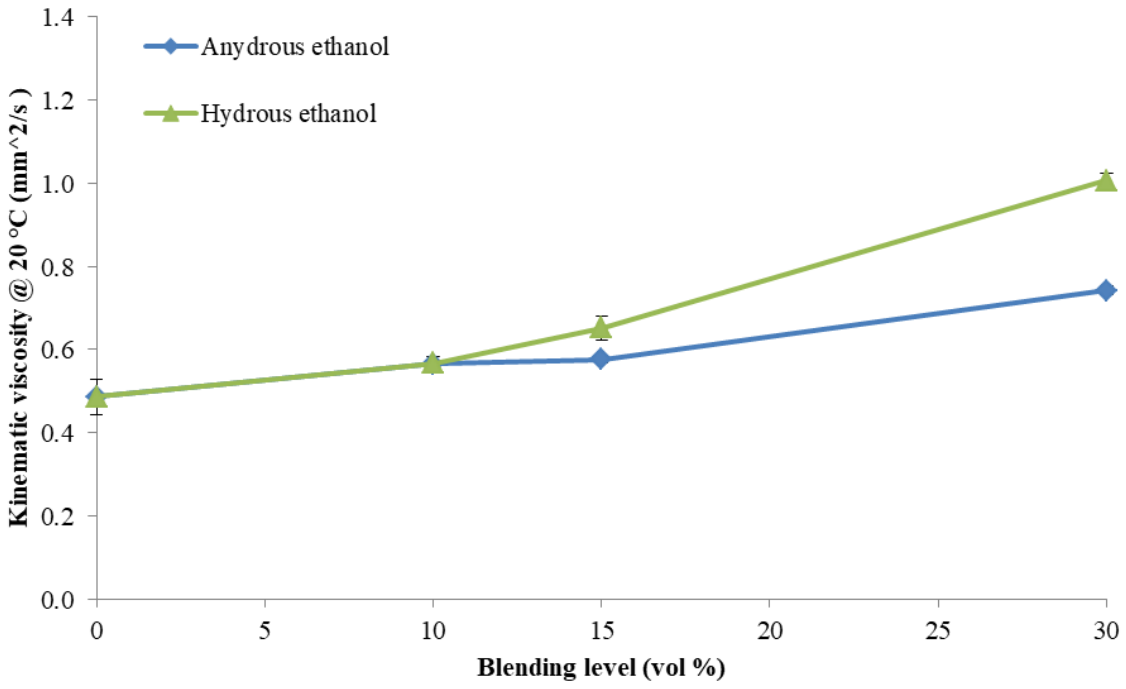

Figure 4.14 Effect of ethanol (anhydrous and hydrous) blending on kinematic viscosity of gasoline. Error bars represent one standard deviation.

4.4 Conclusion

Available thermophysical property data for hydrous ethanol-gasoline blends is sparse. These data are important to evaluate the fuel's potential for use in state of the art vehicle technologies and to optimize engine strategies to maximize engine efficiency. In this study, the distillation curve, Reid vapor pressure, vapor lock index, viscosity, density, copper strip corrosion, haze and phase separation points, and lower heating value of gasoline, hydrous ethanol-gasoline, and anhydrous ethanol-gasoline blends at different volumetric ratios were compared to assess the

substitution potential of hydrous ethanol comprised of the azeotropic proportions of water and ethanol (4: 96 vol % water: ethanol) with blends containing anhydrous ethanol. Results suggested that hydrous ethanol-gasoline blends have the potential to be used in current SI engines as a drop-in fuel with no or only minor changes.

5 Volatility Behavior of Dual-alcohol Blends

5.1 Background

There are limitations with blending low molecular weight alcohols with gasoline. Methanol and ethanol form azeotropes with hydrocarbons compounds in gasoline resulting in a high vapor pressure which can cause evaporative emissions [95]. In addition, low molecular weight alcohols promote phase separation in the presence of water due to their hygroscopicity which can result in a corrosive separated alcohol/water mixtures [20]. In addition, they suffer from low LHV [96]. Furthermore, the high HoV of lower alcohols can cause cold start problems under certain operation conditions [97]. Given the limitations, use of one or more additives may enhance the favorable characteristics while mitigating unwanted behaviors. Higher alcohols (term used to describe any saturated mono-alcohol with higher molecular weight than ethanol) can be a good option for use as a co-solvents with lower alcohols blended with gasoline for several reasons:

(1) Higher alcohols are less corrosive and highly soluble in the gasoline [96].

(2) Higher alcohols increase the water tolerance of alcohol-gasoline blends [98].

(3) Higher alcohols exhibit better lubrication and contribute to less engine wear due to their higher viscosity [20].

(4) Higher alcohols have a higher LHV than lower alcohols [41]

(5) The reduced azeotropic activity of higher alcohols can mitigate evaporation driven concerns associated with lower alcohols [99].

Andersen et al. [12] discussed that it is possible to obtain an alcohol gasoline blend with a Reid vapor pressure (RVP) matching that of the base-gasoline by mixing a lower alcohol and a higher alcohol in gasoline. The objective of this study was to characterize the physiochemical properties, volatility behavior, and mixing/sooting potential of matched RVP dual-alcohol blends

over a wide blending volume range. Subsequently, the results were compared to the corresponding single alcohol-gasoline blends and the neat gasoline. This part was done similar to the Part I (characterization of hydrous ethanol blends), but my role was to focus on the volatility and mixing/sooting potential. The rest of the results are not presented here.

5.2 Test fuels

The base-gasoline used was an unleaded test gasoline (UTG-96) from Phillips 66. Ethanol (200 proof) was obtained from Fisher scientific. Iso-butanol (≥ 99 %, FG) and 3-methyl-3-pentanol (≥ 99 %, FG) were obtained from Sigma-Aldrich. The detailed composition of gasoline obtained in this study is available in the Table 3.1. A total of nine gasoline alcohol blends as well as the neat gasoline were tested in this study. Total alcohol blending volumes spanning from 10 - 40 vol % were considered to investigate the effect of increase alcohol usage on the fuel specifications. All blends are tabulated in Table 5.1. Hereinafter G, E, B, and H represent gasoline, ethanol, iso-butanol, and 3-methyl-3-pentanol, respectively. Since 3-methyl-3-pentanol (3M3P) is an isomer of 1-hexanol (C6 mono-alcohol), it is presented with the letter "H" here. In this chapter, each blend is presented with an alphanumeric code in which the letter (or letters) represents the alcohol (or alcohols) used in the blend and the number represents the total alcohol volume fraction. For instance, E10 consists of 10 vol% ethanol and 90 vol% gasoline while EB40 consists of 40 vol% total alcohol (33.1 vol% ethanol + 6.9 vol% iso-butanol as described in Table 4.1) and 60 vol% gasoline.

Dual-alcohol blends were selected to control the RVP with the intent to reduce the issues associated with the increased volatility of the ethanol blends. The concentration of ethanol and higher alcohols in each dual-alcohol blend was obtained by using the equation proposed by Anderson et al. [12] aiming to match the blend's RVP with that of base-gasoline:

$$C_i = \left(\frac{RVP_G - RVP_j(@C_t)}{RVP_i(@C_t) - RVP_j(@C_t)}\right) \times C_t \quad \text{Eq. 5.1}$$

Where C_i is the volume fraction of alcohol i, C_t is the total alcohol volume fraction, RVP_G is the RVP of the base-gasoline, and $RVP_i(@C_t)$ and $RVP_j(@C_t)$ are RVPs of single alcohols i and j at C_t, respectively. Volumetric concentrations of alcohols for each dual-alcohol blend are indicated in Table 4.1.

Table 5.1 List of test blends. E: ethanol. B: i-butanol. H: 3-methyl-3-pentanol.

Total alcohol volume fraction (vol%)	Ethanol blends	Dual-alcohol blends containing iso-butanol (lower alcohol vol%+ iso-	Dual-alcohol blends containing 3M3P (lower alcohol vol%+3M3P vol%)
10	E10	EB10 (E 2.7 vol% +B 7.3 vol%)	EH10 (E 3.3 vol% +H 6.7 vol%)
20	E20	EB20 (E 8.9 vol% +B 11.1 vol%)	EH20 (E 11.5 vol% +H 8.5 vol%)
40	E40	EB40 (E 33.1 vol% +B 6.9 vol%)	EH40 (E 36.3 vol% +H 3.7 vol%)

5.3 Results and discussion

Vapor pressure: The RVP of all tested gasoline blends are shown in Table 5.2. All dual-alcohol blends exhibited a RVP very close to that of the base-gasoline regardless of total alcohol concentration. Hence, using higher alcohols as co-solvents in blends of gasoline with lower alcohols seems to be a viable option for controlling the RVP that are responsible for evaporative emissions.

Table 5.2 RVP of tested fuels. Values are shown as the mean +/- one standard deviation of triplicate.

Fuel	RVP (kPa)
Gasoline	52.07 ± 0.83
E10	59.63 ± 0.25
EB10	53.44 ± 0.09
EH10	55.89 ± 0.07
E20	58.21 ± 0.41
EB20	53.17 ± 0.16
EH20	54.96 ± 0.18
E40	53.97 ± 0.13
EB40	51.98 ± 0.04
EH40	53.61 ± 0.15

Distillation curve: Distillation curves are obtained at ambient pressure of 84.3 kPa depicted in Figures 5.1 to 5.3. The distillation curve of the unblended gasoline (presented in Figures 5.1-5.2 as a reference point) demonstrates smooth and steadily increasing temperatures. Addition of ethanol to gasoline increases the volatility, through the formation of positive azeotropes, and causes a significant reduction in the front end and midrange distillation temperatures, the extent of which depends on the initial blending fractions of ethanol. For the single ethanol blends, once ethanol evaporates, a relatively sharp rise in boiling temperatures is observed as the distillation curves approach boiling temperatures to that of the gasoline. No significant difference was observed among the initial boiling temperatures of the ethanol blends and gasoline. However, end-point temperatures decrease in the alcohol blends slightly due to the dilution of heavy hydrocarbons.

Distillation curves for the dual-alcohol blends lie between the curves of the corresponding single-alcohol blends. At the beginning of the distillation, temperatures are closer to that of the corresponding ethanol blend while at higher volume fractions, once most of ethanol is evaporated,

there is a sharp rise in boiling temperatures as the distillation curve converges to that of the single-higher alcohol blend.

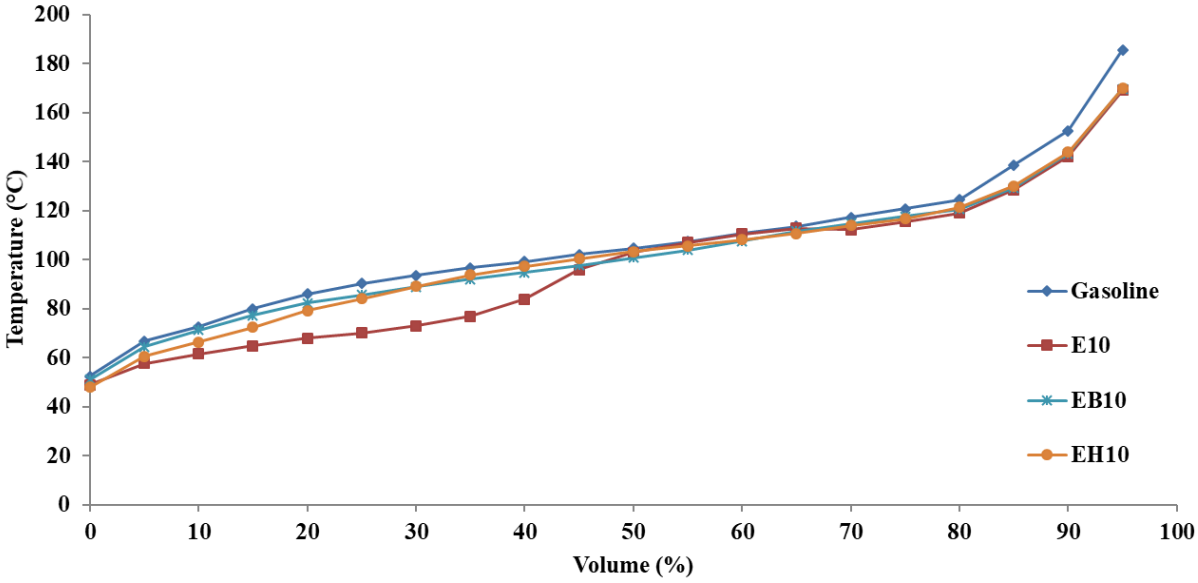

Figure 5.1 Average distillation curves for gasoline and blends containing 10 vol% alcohol. Data was taken at 84.3 kPa. E: ethanol. B: i-butanol. H: 3-methyl-3-pentanol. Average standard error: ± 1.68 °C.

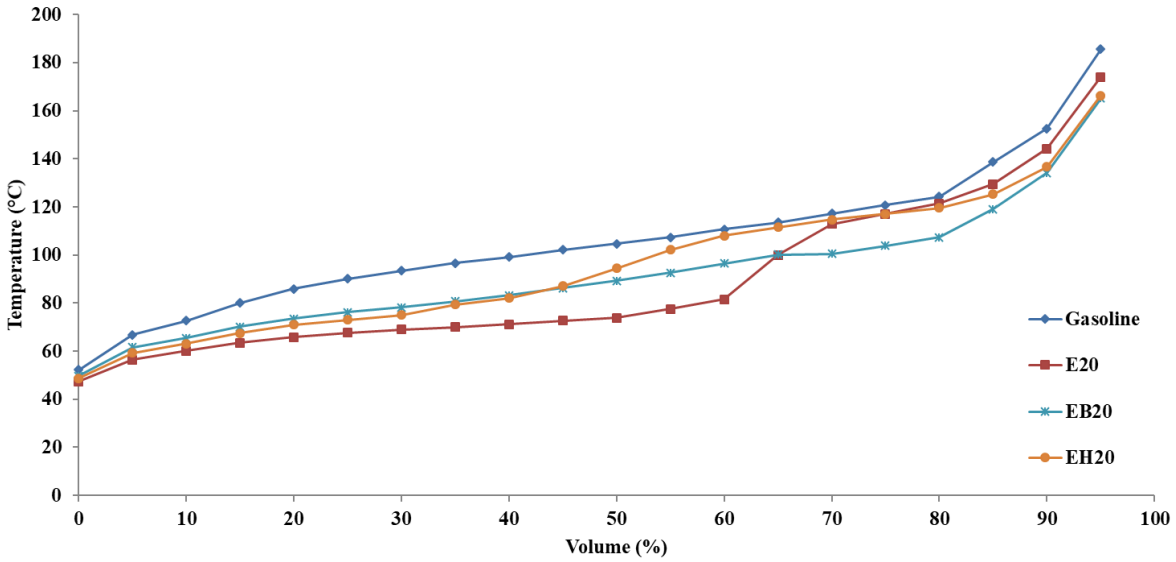

Figure 5.2 Average distillation curves for gasoline and blends containing 20 vol% alcohol. Data was taken at 84.3 kPa. E: ethanol. B: i-butanol. H: 3-methyl-3-pentanol. Average standard error: ± 0.84 °C.

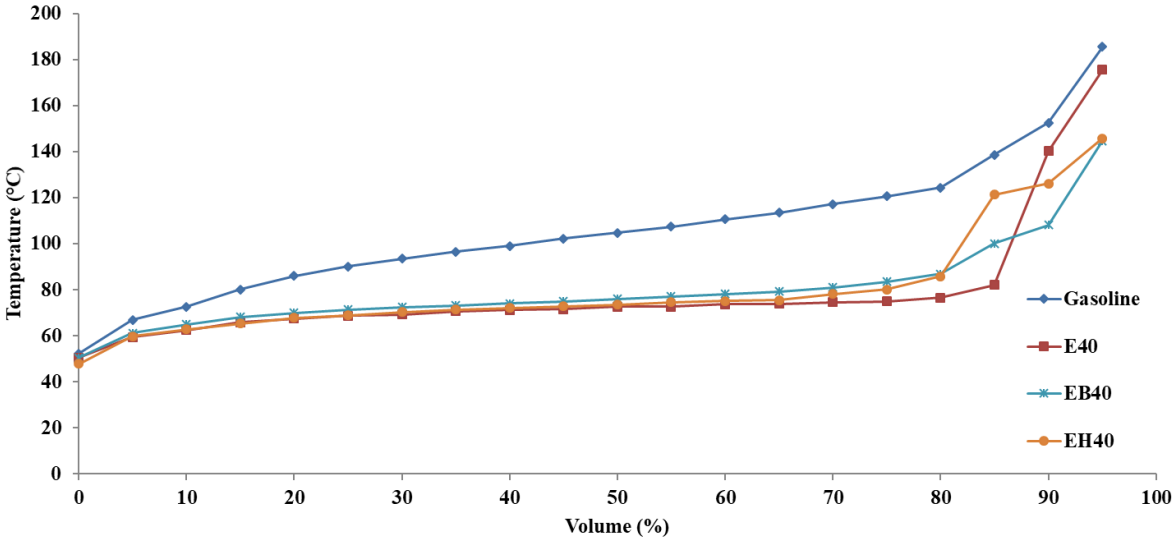

Figure 5.3 Average distillation curves for gasoline and blends containing 40 vol% alcohol. Data was taken at 84.3 kPa. E: ethanol. B: i-butanol. H: 3-methyl-3-pentanol. Average standard error: ± 0.56 °C.

Figure 5.4 shows the distillate oxygenate and aromatic concentrations throughout the distillation process for these blends. It can be inferred from Figure 5.4 that the presence of alcohol(s), especially ethanol, suppress the distillation of aromatic species which is apparent from the sharp rise in aromatic concentration once ethanol is evaporated. The evaporation of aromatics is more delayed for the blends containing higher concentrations of ethanol. This aromatic enrichment occurs because ethanol evaporates initially postponing the evaporation of the heavier aromatics. Given that aromatics generally have shorter kinetic pathways compared to other types of hydrocarbons available in the gasoline [100], there is high possibility of PM formation. It is worth noting that in most cases the mass percentages of aromatics at the late stages of the distillation curve (90% for example) for gasoline are nearly identical to that of the ethanol blends despite the total amount of aromatics is the ethanol blends to be much lower than in the gasoline due to dilution. Comparing the dual-alcohol blends with the single ethanol blends, the blends containing higher alcohols (especially those with 3M3P) minimize the suppression and result in less aromatic concentrations at the 90% volume distilled point especially at higher blending ratios.

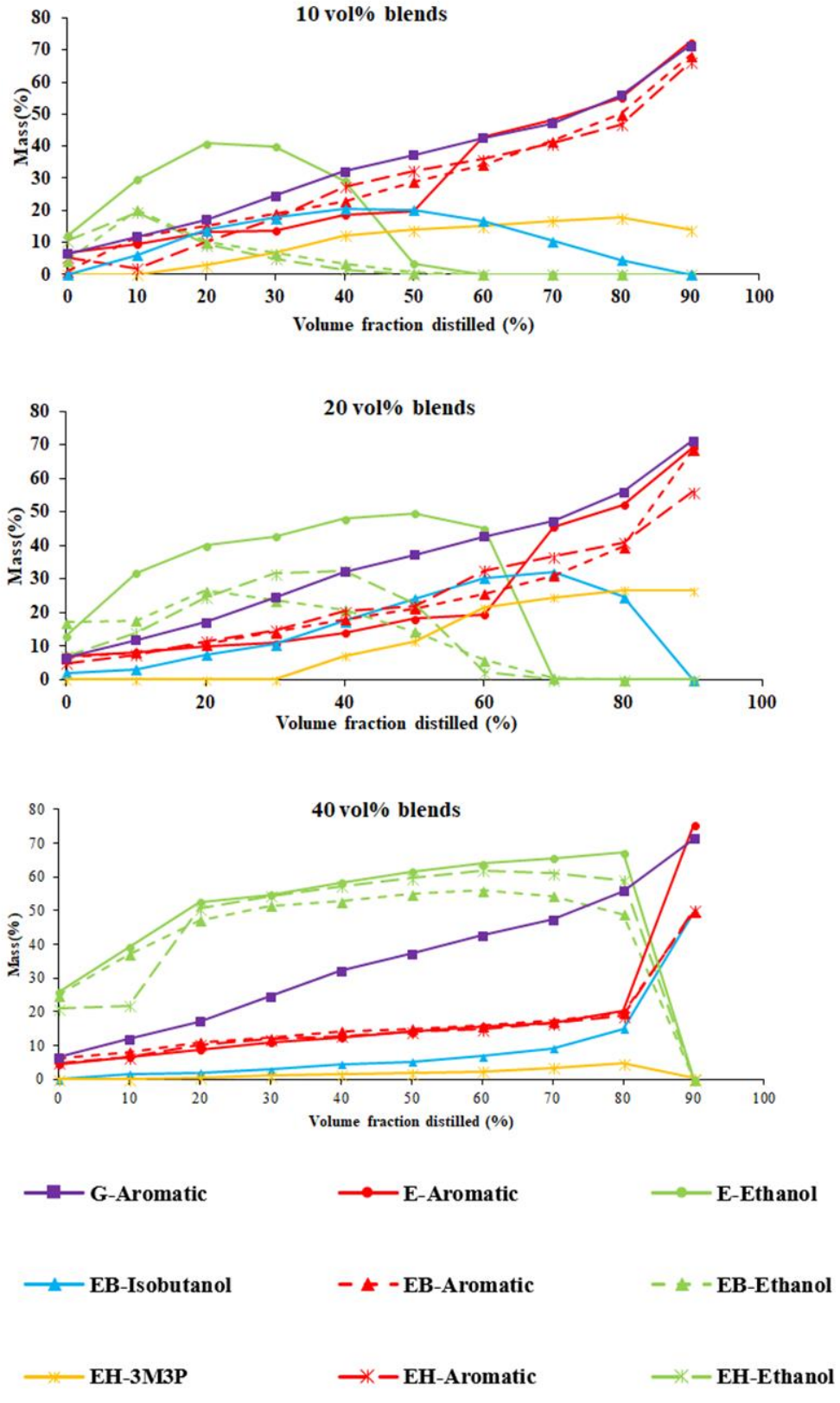
10 vol% blends
Mass(%)
Volume fraction distilled (%)
20 vol% blends
Mass(%)
Volume fraction distilled (%)
40 vol% blends
Mass(%)
Volume fraction distilled (%)
G-Aromatic
E-Aromatic
E-Ethanol
EB-Isobutanol
EB-Aromatic
EB-Ethanol
EH-3M3P
EH-Aromatic
EH-Ethanol

Figure 5.4 Detailed hydrocarbon analysis results of the distillate collected during distillation. The average coefficient of variations of the data was calculated to be ±2.51% for aromatics and ±3.66% for oxygenates. G-Aromatic: Mass percent of aromatics in gasoline. E-Aromatic: Mass percent of aromatics in ethanol blends. EB-Aromatic: Mass percent of aromatics in dual-alcohol blends containing i-butanol. EH-Aromatic: Mass percent of aromatics in dual-alcohol blends containing 3M3P. E-Ethanol: Mass percent of ethanol in ethanol blends. EB-Ethanol: Mass percent of aromatics in dual-alcohol blends containing i-butanol. EH-Ethanol: Mass percent of aromatics in dual-alcohol blends containing 3M3P. EB- Isobutanol: Mass percent of i-butanol in dual-alcohol blends containing i-butanol. EH-3M3P: Mass percent of 3M3P in dual-alcohol blends containing 3M3P.

Distillation model: As seen in Figure 5.5, the model is accurately predicting the temperature inflection points for each of the mixtures and the corresponding composition changes as evident by the positive agreement between the predicted and measured molecular weights demonstrated in Figure 5.6. The overall agreement demonstrates the accuracy of the distillation model providing confidence that VLE is accurately captured and can be used to predict droplet evaporation. [74].

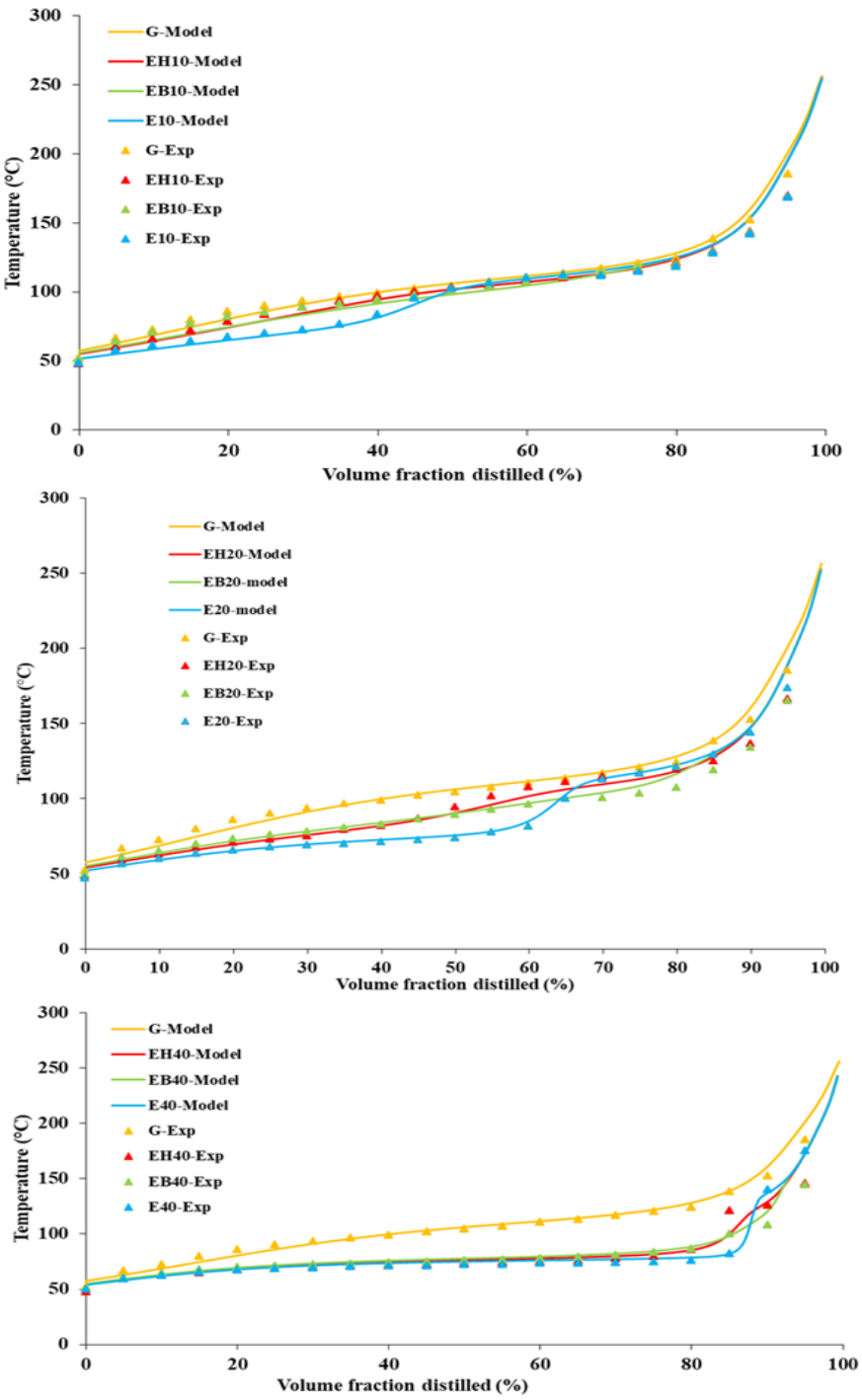

Figure 5.5 Comparison of experimentally measured and predicted distillation curves. Exp: experimentally measured average molecular weight. Model: predicted average molecular weight. G: gasoline. E: ethanol. B: i-butanol. H: 3-methyl-3-pentanol.

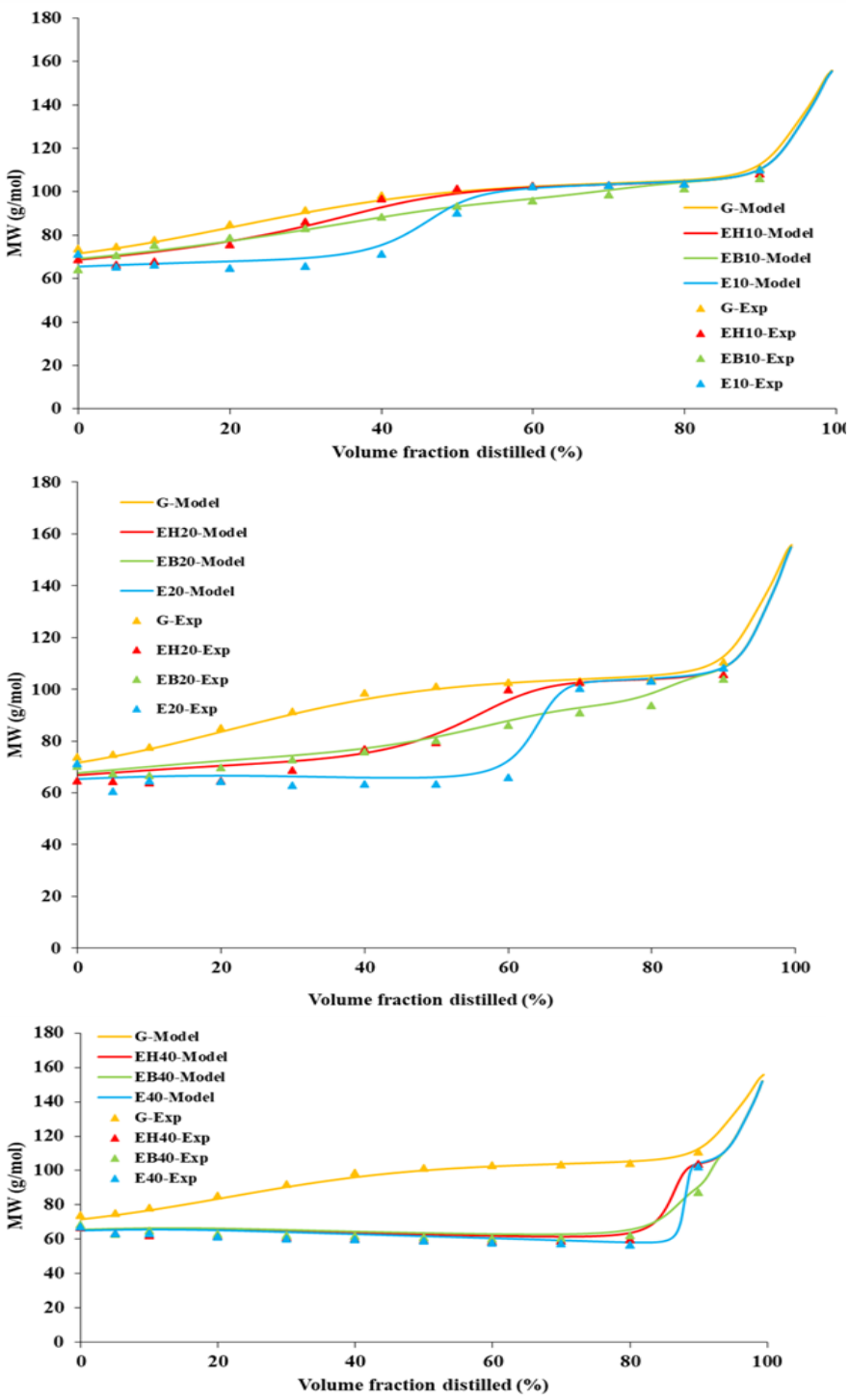

Figure 5.6 Comparison of experimentally measured and predicted average molecular weight. Exp: experimentally measured average molecular weight. Model: predicted average molecular weight. G: gasoline. E: ethanol. B: i-butanol. H: 3-methyl-3-pentanol.

Droplet evaporation model: Alcohols (especially higher alcohols) increase the viscosity and density of blends especially at medium and high blending ratios which can result in the formation of large size droplets sizes and subsequently higher PM exhaust emissions [43]. To take these physical properties into account, as explained in section 4.3.1.4.2, Eq. 4.4 was used to estimate the droplet size of all the fuel blends when initial droplet size of gasoline was assumed to be 25 μm. The calculated droplets sizes for each blend are listed in Table 5.3. The droplet evaporation model was then run with the calculated initial droplet sizes for each blend at constant ambient temperature (323 K) and atmospheric pressure to determine the influence of droplet size on droplet evaporation lifetimes.

Figure 5.7 shows that alcohols increase the HOV of the mixture which is more observable in blends with higher blending ratios of alcohols. Ethanol blends exhibit a slightly higher transient HoV when compared to the dual counterpart, resulting from the higher HoV of ethanol compared to the higher alcohols, as shown in Table 5.4. However, this only translates into a minor difference in the minimum droplet temperature between the ethanol and dual-alcohol mixtures as seen in Figure 5.8. In general, the presence of oxygenates results in a greater initial temperature drop compared to the neat gasoline. The HoV and temperature remain high and low, respectively, until ethanol and the higher alcohol are evaporated. The total oxygenate concentration profiles are shown in Figure 5.9 for all blends. After depletion of oxygenates, temperature and HoV of all droplets converge with that of gasoline.

Figure 5.10 shows that dual-alcohol blends exhibited longer droplet evaporation times compared to gasoline regardless of total alcohol concentration despite having similar RVP values as a result of higher HoV and larger initial droplet sizes. This difference is more accentuated for blends with higher blending ratios due to the larger HoV and droplet sizes. Among the dual-alcohol

blends, those containing iso-butanol experienced slower evaporation because of the higher HoV of iso-butanol relative to 3M3P. The only oxygenated blend that exhibited shorter evaporation time than gasoline is E10, which can be attributed to the blend's high vapor pressure. In the case of E20 and E40, the reduced RVP, increased HoV, and increase in droplet size compared to E10 lead to longer evaporation times relative to gasoline. Comparing dual-alcohol blends with ethanol blends, ethanol blends show shorter evaporation time compared to corresponding dual- alcohols because of higher volatility regardless of slightly higher HoV. The only exception is E40 which has a longer evaporation time than EH40 because of the difference in HoV between E40 and EH40 is high enough to overcome the differences in volatility. Interestingly, this is not the case with EB40 because iso-butanol has a higher HoV than 3M3P. These results indicate that once accounting for the multiple changes in properties responsible for droplet atomization and vaporization fuels containing alcohol(s) may in fact possess slower in-cylinder evaporation behaviors and as a result potentially more prone to form inhomogeneous charges that could contribute to PM emissions.

Table 5.3 Physical properties and corresponding droplet sizes obtained from Elkotb model [90] for test fuels

Fule	ρ (g/cm^3)	Surface tension [a] (N/m)	ν (mm^2/s)	Initial droplet size (µm)
Gasoline	0.74	0.0228	0.50	25.00
E10	0.74	0.0227	0.53	25.71
EB10	0.75	0.0228	0.58	26.91
EH10	0.75	0.0228	0.59	27.12
E20	0.75	0.0227	0.62	27.52
EB20	0.75	0.0227	0.68	28.56
EH20	0.75	0.0228	0.64	27.94
E40	0.77	0.0225	0.88	31.96
EB40	0.77	0.0226	0.94	32.80
EH40	0.76	0.0226	0.85	31.27

[a] Obtained from [93].

Table 5.4 HoV of pure alcohols obtained from [88] [a]

Alcohol	HoV at 25 °C (kJ/kg) [a]
Ethanol	924.1
Iso-butanol	701.9
3-methyl-3-pentanol	474.0

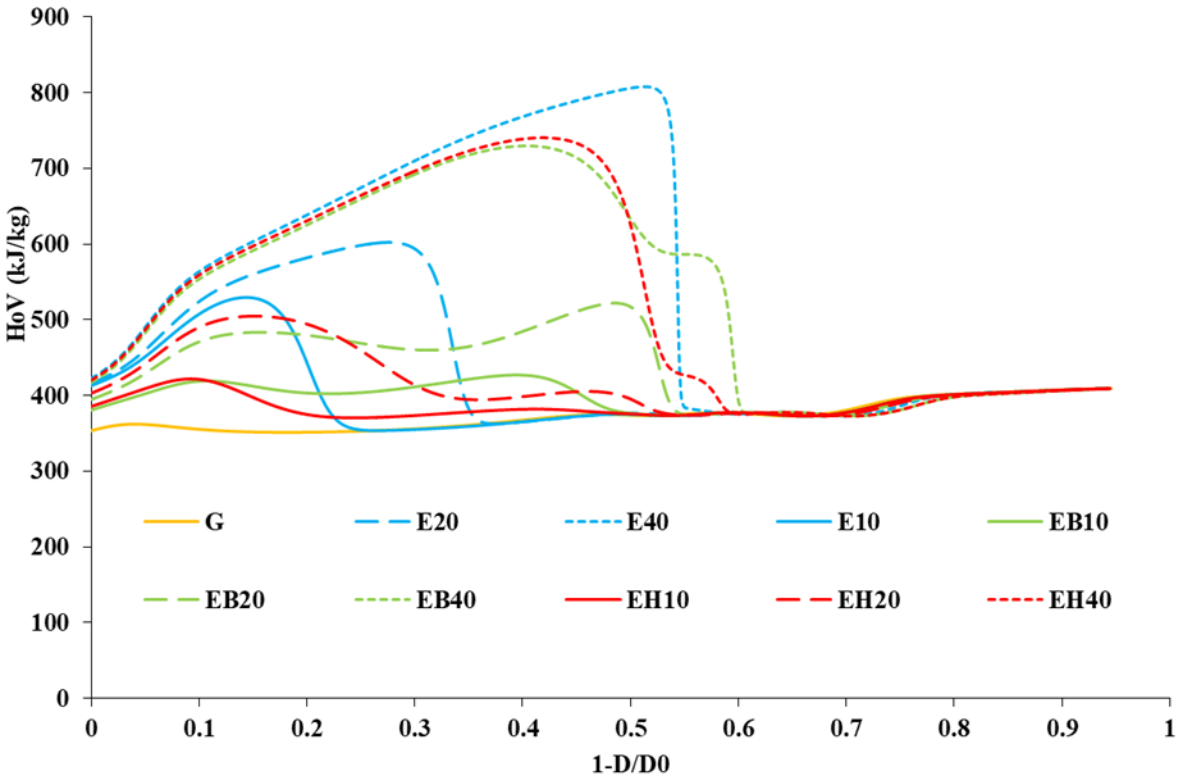

Figure 5.7 HoV profiles of gasoline and the alcohol blends obtained from the droplet evaporation model as a function of droplet diameter regression when subjected to a constant ambient pressure and temperature of 1 atm and 323 K, respectively. G: gasoline. E: ethanol. B: i-butanol. H: 3-methyl-3-pentanol. D: Diameter. D0: Initial diameter.

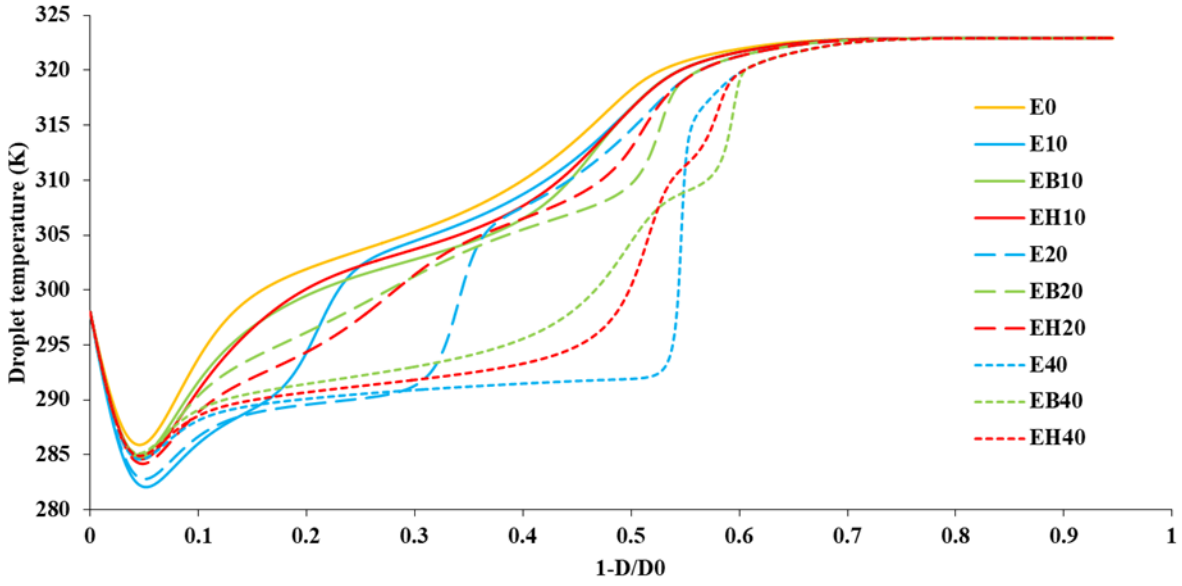

Figure 5.8 Temperature profiles of gasoline and alcohol blends obtained from droplet evaporation model as a function of droplet regression when subjected to a constant ambient pressure and temperature of 1 atm and 323 K, respectively. G: gasoline. E: ethanol. B: i-butanol. H: 3-methyl-3-pentanol. D: Diameter. D0: Initial diameter.

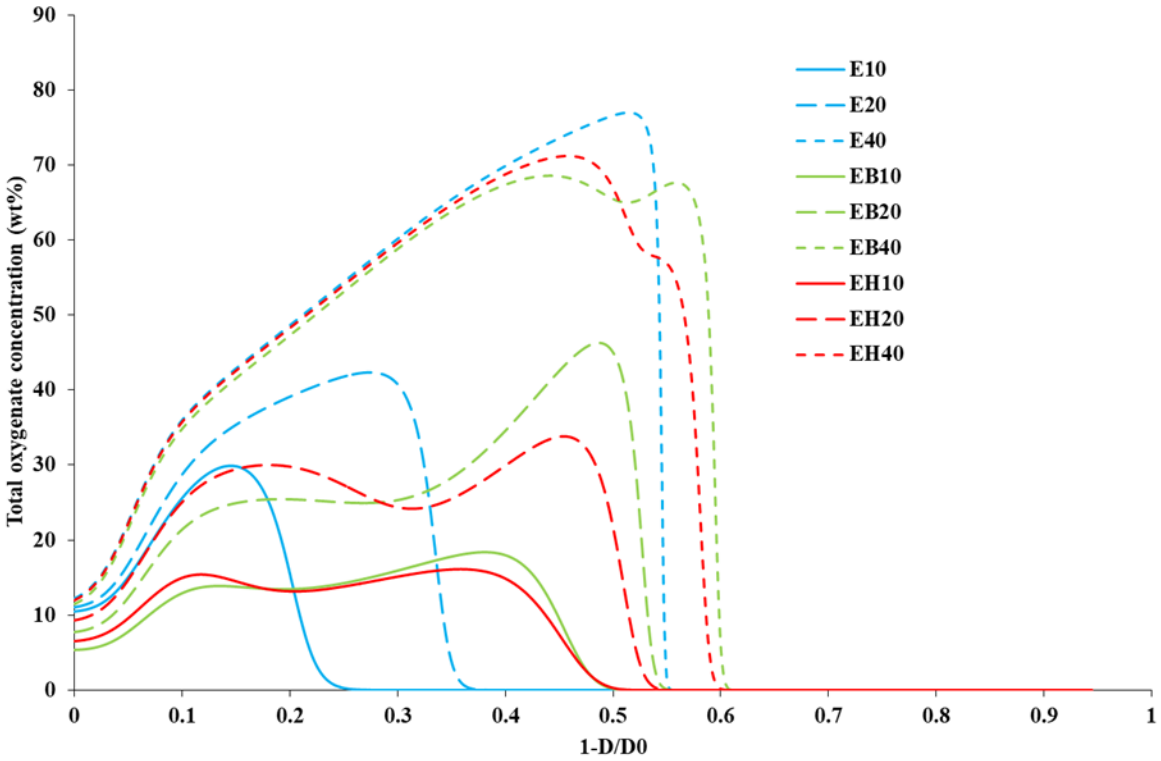

Figure 5.9 Total oxygenate concentration profiles from droplet evaporation model as a function of droplet regression when subjected to a constant ambient pressure and temperature of 1 atm and 323 K, respectively. E: ethanol. B: i-butanol. H: 3-methyl-3-pentanol

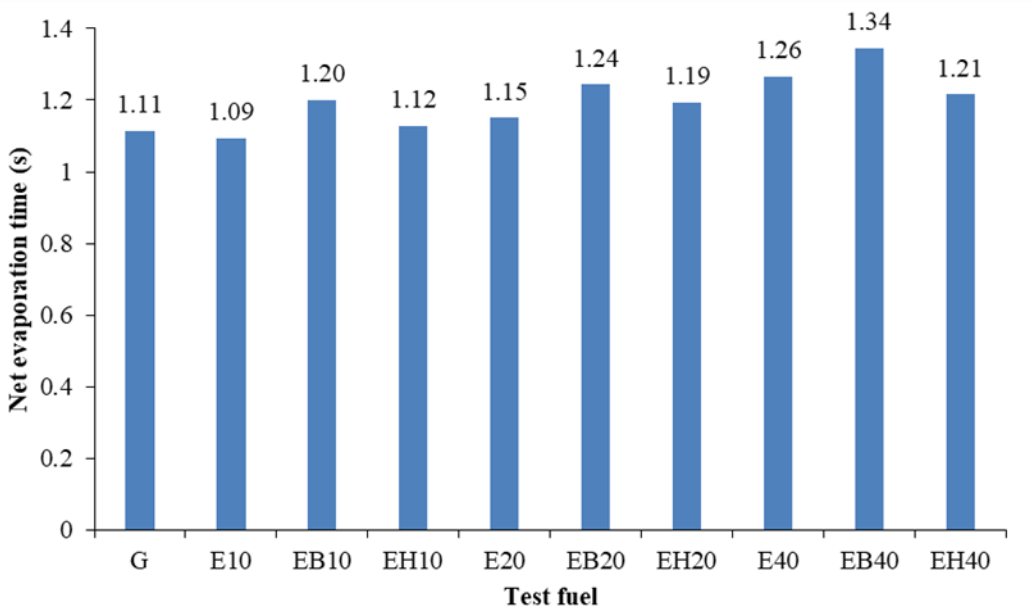

Figure 5.10 Droplet evaporation time for gasoline and alcohol blends obtained from droplet evaporation model for a constant ambient pressure and temperature of 1 atm and 323 K, respectively.

5.4 Conclusion

In this part of project, it was observed that dual-alcohol blends could successfully keep the RVP very close to that of gasoline, which can mitigate limitations associated with low and high volatilities. Composition evolution during the distillation revealed that the presence of alcohols suppresses the evaporation of the aromatic species which are well-known soot precursors. Furthermore, results of droplet evaporation model showed that alcoholic blends have longer droplet life-times compared to gasoline despite having similar vapor pressure in case of dual-alcohol blends because of higher HoV and larger droplet sizes.

6 Conclusions and Recommendations

6.1 Part I: Hydrous ethanol-gasoline mixtures

The physiochemical properties and volatility of gasoline blended with hydrous and anhydrous ethanol at different volumetric ratios were studied to assess the substitution potential of hydrous ethanol, comprised of the azeotropic proportions of water and ethanol, to circumvent high energy costs associated with the current production of anhydrous ethanol fuel. Distillation curve, Reid vapor pressure, vapor lock index, viscosity, density, copper strip corrosion, haze and phase separation points, and lower heating value were measured for all samples. The composition evolution of the unblended gasoline and the oxygenated blends during the distillation was measured by sampling and analyzing the condensate samples throughout the distillation process. Furthermore, the droplet evaporation model was exploited to understand how non-ideal volatility behavior of these blends can inhibit complete fuel-air mixing and potentially contribute to soot formation in direct injection systems. The primary outcomes of this work are listed here:

- Differences in LHV were not significant between hydrous and anhydrous blends even at blending ratios of 30% by volume.
- Presence of water increased the viscosity and density especially at higher blending concentration which may be problematic due to the formation of larger droplets resulting in slower atomization/evaporation dynamics.
- Phase separation occurred at relatively high temperatures for hydrous ethanol blends especially for the low and medium blending levels (i.e. 10% and 15%) indicating that the use of additive for preventing phase separation may be necessary. Interestingly, the high

blending ratio hydrous ethanol mixtures (i.e. 30 %) exhibited phase separation at much lower temperatures than the 10 and 15% blends despite having a higher total water content.

- Experimental data shows that the addition of both anhydrous and hydrous ethanol into gasoline can cause a significant reduction in boiling temperatures of the distillation curve depending on the initial concentration. However, at each blending ratio, hydrous and anhydrous ethanol blends presented similar trends with negligible observed differences in boiling temperatures.
- Having compared experimental results with ASTM D4814 specifications, all oxygenated blends were qualified at least for one of the vapor pressure/distillation classes although gasoline itself could not pass the T10 requirement.
- Analysis of the distillate samples revealed that ethanol and water suppress the evaporation of the aromatic species, which are well-known soot precursors, to later in the distillation curve, however, again, no significant difference was observed between hydrous and anhydrous blends in the distillate aromatic composition.
- Results from droplet evaporation simulations showed that with modified droplet sizes based on the measured and predicted physical properties of the fuel blends, the presence of oxygenates led to longer droplet evaporation times than gasoline (E0) as a result of larger initial droplet sizes. Comparing hydrous blends with anhydrous blends, while accounting for variation in droplet sizes, the higher HoV and viscosity of water relative to ethanol can play a significant role leading to notable differences in the net evaporation time between the hydrous and anhydrous blends especially at moderate to high blending ratios.

These results suggest that without updates to the fuel injection system, the utilization of water (i.e. hydrous ethanol) may extend droplet lifetimes. Taking these results into account, it can be

concluded that at low engine speeds in which there is enough time for evaporation, there may be no notable difference between gasoline and the other blends in terms of PM emissions, however, at some engine conditions (e.g. very high loads and speeds) there may not be enough time for complete droplet evaporation, which would increase the probability of fuel spray impingement on the cylinder walls in a DISI platform. This slowed evaporation coupled with the suppression of the aromatics' evaporation by ethanol and water may cause higher PM emissions relative to gasoline. Therefore, to investigate the potential of spray impingement/pool burning responsible for increased PM, further research including spray characterization experiments and engine testing/PM measurements is suggested. In addition, it is recommended that future work be conducted on the characterization of fuels with higher water/ethanol ratios, compatibility of fuel delivery/storage systems and economical/energy life cycle aspects of replacing hydrous ethanol with anhydrous ethanol to examine potential of hydrous ethanol- gasoline mixtures as fuel blends.

6.2 Part II: Dual-alcohol blending approach

Six dual-alcohol blends with a matched RVP to gasoline and corresponding ethanol blends were characterized in terms of volatility behavior and mixing/sooting potential of matched RVP dual-alcohol blends over a wide blending volume range by using distillation measurements and droplet evaporation model.

- Regardless of total alcohol concentration, dual-alcohol blends successfully kept the RVP very close to that of gasoline and addressed limitations associated with high volatility for blends containing low to medium concentrations of single lower alcohols in addition to low volatility concerns for blends containing medium to high concentrations of single higher alcohols.

- Distillation curves of dual-alcohol blends lie between the curves of the corresponding single-alcohol blends. At the beginning, the distillation curves are relatively close to the ethanol blend. After the evaporation of the ethanol which occurs at a temperature close to its boiling point, the distillation curve approaches the corresponding single-higher alcohol blend at a temperature close to the boiling point of the higher alcohol.
- Composition evolution during the distillation revealed that the presence of alcohols suppresses the evaporation of the aromatic species which are well-known soot precursors.
- Results of droplet evaporation model showed that alcoholic blends have longer droplet life-times compared to gasoline despite having similar vapor pressure. In the case of dual-alcohol blends this occurs as a result of their higher HoV and larger initial droplet sizes.

The results of this study showed that it is advantageous to use dual-alcohol blends as they contain more portion of biofuel and may offer better properties than single alcohol blends necessary for good performance in existing spark-ignition engines.

This research can be further continued with characterizing physiochemical properties of these fuels, identification of combustion/emissions characteristics and research that supports economical production processes for higher alcohols.

7 References

1- Reddy HK, Muppaneni T, Rastegary J, Shirazi SA, Ghassemi A, Deng S. ASI: Hydrothermal extraction and characterization of bio-crude oils from wet chlorella sorokiniana and dunaliella tertiolecta. Environ Prog Sustain Energy 2013;32:910–5. doi:10.1002/ep.11862.

2- Environmental Protection Agency. Renewable Fuel Standard Program (RFS2) Regulatory Impact Analysis. 2010. doi:EPA-420-R-10-006., February 2010.

3- Independent Statistics & Analysis (EIA). Electric Power Monthly: with data for January 2016. US Energy Inf Adm 2016:237. doi:10.2172/123200.

4- Cardona CA, Sánchez ÓJ. Fuel ethanol production: Process design trends and integration opportunities. Bioresour Technol 2007;98:2415–57. doi:10.1016/j.biortech.2007.01.002.

5- Shapouri H, Duffield JA, Wang M. The energy balance of corn ethanol revisited. Trans ASAE 2003;46:959–68. doi:10.1016/j.enpol.2006.02.007.

6- Lide DR. CRC Handbook of Chemistry and Physics, 84th Edition, 2003-2004. Handb Chem Phys 2003;53:2616. doi:10.1136/oem.53.7.504.

7- Dean JA. Lange's handbook of chemistry. Mater Manuf Process 1990;5:687–8. doi:10.1080/10426919008953291.

8- Munsin R, Laoonual Y, Jugjai S, Imai Y. An experimental study on performance and emissions of a small SI engine generator set fuelled by hydrous ethanol with high water contents up to 40%. Fuel 2013;106:586–92. doi:10.1016/j.fuel.2012.12.079.

9- Lawson KW, Lloyd DR. Membrane distillation. J Memb Sci 1997;124:1–25. doi:10.1016/S0376-7388(96)00236-0.

10- Pacheco-Basulto J ángel, Hernández-McConville D, Barroso-Muñoz FO, Hernández S, Segovia-Hernández JG, Castro-Montoya AJ, et al. Purification of bioethanol using extractive

batch distillation: Simulation and experimental studies. Chem Eng Process Process Intensif 2012;61:30–5. doi:10.1016/j.cep.2012.06.015.

11- ASTM D4814-17 Standard Specification for Automotive Spark-Ignition Engine Fuel, West Conshohocken, PA, 2017, https://doi.org/10.1520/D4814-17

12- Andersen VF, Anderson JE, Wallington TJ, Mueller SA, Nielsen OJ. Vapor pressures of alcohol-gasoline blends. Energy and Fuels, vol. 24, 2010, p. 3647–54. doi:10.1021/ef100254w.

13- Siwale L, Kristóf L, Bereczky A, Mbarawa M, Kolesnikov A. Performance, combustion and emission characteristics of n-butanol additive in methanol-gasoline blend fired in a naturally-aspirated spark ignition engine. Fuel Process Technol 2014;118:318–26. doi:10.1016/j.fuproc.2013.10.007.

14- Ratcliff MA, Luecke J, Williams A, Christensen E, Yanowitz J, Reek A, et al. Impact of higher alcohols blended in gasoline on light-duty vehicle exhaust emissions. Environ Sci Technol 2013;47:13865–72. doi:10.1021/es402793p.

15- Mainguet SE, Liao JC. Bioengineering of microorganisms for C3 to C5 alcohols production. Biotechnol J 2010;5:1297–308. doi:10.1002/biot.201000276.

16- Westbrook CK. Biofuels Combustion. Annu Rev Phys Chem 2013;64:201–19. doi:10.1146/annurev-physchem-040412-110009.

17- Demirbas A. Biofuels securing the planet's future energy needs. Energy Convers Manag 2009;50:2239–49. doi:10.1016/j.enconman.2009.05.010.

18- Perlack RD, Wright LL, Turhollow AF, Graham RL, Stokes BJ, Erbach DC. Biomass as Feedstock for a Bioenergy and Bioproducts Industry : The Technical Feasibility of a Billion-Ton Annual Supply. Agriculture 2005;DOE/GO-102:78. doi:10.2172/885984.

19- Lee SK, Chou H, Ham TS, Lee TS, Keasling JD. Metabolic engineering of microorganisms for biofuels production: from bugs to synthetic biology to fuels. Curr Opin Biotechnol 2008;19:556–63. doi:10.1016/j.copbio.2008.10.014.

20- Surisetty VR, Dalai AK, Kozinski J. Alcohols as alternative fuels: An overview. Appl Catal A Gen 2011;404:1–11. doi:10.1016/j.apcata.2011.07.021.

21- Panwar NL, Kothari R, Tyagi V V. Thermo chemical conversion of biomass - Eco friendly energy routes. Renew Sustain Energy Rev 2012;16:1801–16. doi:10.1016/j.rser.2012.01.024.

22- Narayanasamy M, Hashim H, Yunus NA. Computational and Experimental Investigations on Tailor-made Biofuel Blend Properties. Energy Procedia, vol. 75, 2015, p. 23–9. doi:10.1016/j.egypro.2015.07.130.

23- Bergthorson JM, Thomson MJ. A review of the combustion and emissions properties of advanced transportation biofuels and their impact on existing and future engines. Renew Sustain Energy Rev 2015;42:1393–417. doi:10.1016/j.rser.2014.10.034.

24- Li H, Cann AF, Liao JC. Biofuels: Biomolecular Engineering Fundamentals and Advances. Annu Rev Chem Biomol Eng 2010;1:19–36. doi:10.1146/annurev-chembioeng-073009-100938.

25- Dahmen M, Marquardt W. Model-Based Design of Tailor-Made Biofuels. Energy and Fuels 2016;30:1109–34. doi:10.1021/acs.energyfuels.5b02674.

26- Sims REH, Mabee W, Saddler JN, Taylor M. An overview of second generation biofuel technologies. Bioresour Technol 2010;101:1570–80. doi:10.1016/j.biortech.2009.11.046.

27- Borgwardt RH. Transportation fuel from cellulosic biomass: a comparative assessment of ethanol and methanol options. Proc Inst Mech Eng Part A J Power Energy 2005;213:399–407. doi:10.1243/0957650991537770.

28- Nigam PS, Singh A. Production of liquid biofuels from renewable resources. Prog Energy Combust Sci 2011;37:52–68. doi:10.1016/j.pecs.2010.01.003.

29- Peralta-Yahya PP, Keasling JD. Advanced biofuel production in microbes. Biotechnol J 2010;5:147–62. doi:10.1002/biot.200900220.

30- Alonso DM, Bond JQ, Dumesic JA. Catalytic conversion of biomass to biofuels. Green Chem 2010;12:1493. doi:10.1039/c004654j.

31- Patil V, Tran KQ, Giselrød HR. Towards sustainable production of biofuels from microalgae. Int J Mol Sci 2008;9:1188–95. doi:10.3390/ijms9071188.

32- United-States-Environmental-Protection-Agency. Effects of acid rain. Available: ⟨http://www.epa.gov/acidrain/effects/index.html⟩ [11.03.16].

33- Kohse-Höinghaus K, Oßwald P, Cool TA, Kasper T, Hansen N, Qi F, et al. Biofuel combustion chemistry: From ethanol to biodiesel. Angew Chemie - Int Ed 2010;49:3572–97. doi:10.1002/anie.200905335.

34- Agency for Toxic Substances and Disease Registry (ATSDR). Toxicity of Polycyclic Aromatic Hydrocarbons (PAHs). 2009.

35- Gautam M, Martin DW. Combustion characteristics of higher-alcohol/gasoline blends. Proc Inst Mech Eng Part A J Power Energy 2000;214:497–511. doi:10.1243/0957650001538047.

36- Westbrook CK, Pitz WJ, Curran HJ. Chemical kinetic modeling study of the effects of oxygenated hydrocarbons on soot emissions from diesel engines. J Phys Chem A 2006;110:6912–22. doi:Doi 10.1021/Jp056362g.

37- Kirchstetter TW, Singer BC, Harley RA, Kendall GR, Ghan W. Impact of oxygenated gasoline use on California light-duty vehicle emissions. Environ Sci Technol 1996;30:661–70. doi:10.1021/es950406p.

38- United-States-Environmental-Protection-Agency. Substantially similar interpretive rules for fuels and fuel additives under the Clean Air Act. Available: ⟨ https://www.epa.gov/fuels-registration-reporting-and-compliance-help/substantially-similar-interpretive-rules-fuels-and⟩ [11.09.16].

39- Gravalos I, Moshou D, Gialamas T, Xyradakis P, Kateris D, Tsiropoulos Z. Emissions characteristics of spark ignition engine operating on lower higher molecular mass alcohol blended gasoline fuels. Renew Energy 2013;50:27–32. doi:10.1016/j.renene.2012.06.033.

40- Cheng W-H, Kung HH. Methanol production and use. vol. 32. 1994. doi:10.5860/CHOICE.32-3898.

41- Wallner T, Ickes A, Lawyer K. Analytical assessment of C2-C8 alcohols as spark-ignition engine fuels. Lect. Notes Electr. Eng., vol. 191 LNEE, 2013, p. 15–26. doi:10.1007/978-3-642-33777-2_2.

42- Gautam M, Martin DW, Carder D. Emissions characteristics of higher alcohol/gasoline blends. Proc Inst Mech Eng Part A J Power Energy 2000;214:165–82. doi:10.1243/0957650001538263.

43- Lapuerta M, García-Contreras R, Campos-Fernández J, Dorado MP. Stability, lubricity, viscosity, and cold-flow properties of alcohol-diesel blends. Energy and Fuels 2010;24:4497–502. doi:10.1021/ef100498u.

44- Zhao F, Lai MC, Harrington DL. Automotive spark-ignited direct-injection gasoline engines. Prog Energy Combust Sci 1999;25:437–562. doi:10.1016/S0360-1285(99)00004-0.

45- Yao M, Zheng Z, Liu H. Progress and recent trends in homogeneous charge compression ignition (HCCI) engines. Prog Energy Combust Sci 2009;35:398–437. doi:10.1016/j.pecs.2009.05.001.

46- Reitz RD. Directions in internal combustion engine research. Combust Flame 2013;160:1–8. doi:10.1016/j.combustflame.2012.11.002.

47- Kirk-Othmer. Encyclopedia of Chemical Technology. Kirk-Othmer Encycl Chem Technol 2006:944.

48- Alkidas AC. Combustion advancements in gasoline engines. Energy Convers Manag 2007;48:2751–61. doi:10.1016/j.enconman.2007.07.027.

49- Eyidogan M, Ozsezen AN, Canakci M, Turkcan A. Impact of alcohol-gasoline fuel blends on the performance and combustion characteristics of an SI engine. Fuel 2010;89:2713–20. doi:10.1016/j.fuel.2010.01.032.

50- Costagliola MA, De Simio L, Iannaccone S, Prati M V. Combustion efficiency and engine out emissions of a S.I. engine fueled with alcohol/gasoline blends. Appl Energy 2013;111:1162–71. doi:10.1016/j.apenergy.2012.09.042.

51- Watson GMG, Versailles P, Bergthorson JM. NO formation in premixed flames of C1–C3 alkanes and alcohols. Combust Flame 2016;169:242–60. doi:10.1016/j.combustflame.2016.04.015.

52- Williams P, Inman D. Environmental and Sustainability Factors Associated With Next-Generation Biofuels in the U . S .: What Do We Really Know ? Environ Sci Technol 2009;43:4763–75. doi:10.1021/es900250d.

53- Serinyel Z, Black G, Curran HJ, Simmie JM. A shock tube and chemical kinetic modeling study of methy ethyl ketone oxidation. Combust Sci Technol 2010;182:574–87. doi:10.1080/00102200903466129.

54- Lynd LR. OVERVIEW AND EVALUATION OF FUEL ETHANOL FROM CELLULOSIC BIOMASS: Technology, Economics, the Environment, and Policy. Annu Rev Energy Environ 1996;21:403–65. doi:10.1146/annurev.energy.21.1.403.

55- Schifter I, Diaz L, Gómez JP, Gonzalez U. Combustion characterization in a single cylinder engine with mid-level hydrated ethanol-gasoline blended fuels. Fuel, vol. 103, 2013, p. 292–8. doi:10.1016/j.fuel.2012.06.002.

56- Foong TM, Morganti KJ, Brear MJ, da Silva G, Yang Y, Dryer FL. The Effect of Charge Cooling on the RON of Ethanol/Gasoline Blends. SAE Int J Fuels Lubr 2013;6:2013-01–0886. doi:10.4271/2013-01-0886.

57- Kyriakides A, Dimas V, Lymperopoulou E, Karonis D, Lois E. Evaluation of gasoline-ethanol-water ternary mixtures used as a fuel for an Otto engine. Fuel 2013;108:208–15. doi:10.1016/j.fuel.2013.02.035.

58- Costa RC, Sodré JR. Hydrous ethanol vs. gasoline-ethanol blend: Engine performance and emissions. Fuel 2010;89:287–93. doi:10.1016/j.fuel.2009.06.017.

59- Melo TCC De, MacHado GB, Belchior CRP, Colaço MJ, Barros JEM, De Oliveira EJ, et al. Hydrous ethanol-gasoline blends - Combustion and emission investigations on a Flex-Fuel engine. Fuel 2012;97:796–804. doi:10.1016/j.fuel.2012.03.018.

60- Wang X, Chen Z, Ni J, Liu S, Zhou H. The effects of hydrous ethanol gasoline on combustion and emission characteristics of a port injection gasoline engine. Case Stud Therm Eng 2015;6:147–54. doi:10.1016/j.csite.2015.09.007.

61- UTG-96 (unleaded test gasoline) n.d. http://www.cpchem.com/bl/specchem/en-us/Pages/UTG96unleadedtestgasoline.aspx (accessed May 2, 2018).

62- ASTM D130-12 Standard Test Method for Corrosiveness to Copper from Petroleum Products by Copper Strip Test, West Conshohocken, PA, 2012, https://doi.org/10.1520/D0130-12

63- ASTM D6422-99 Standard Test Method for Water Tolerance (Phase Separation) of Gasoline-Alcohol Blends Test, West Conshohocken, PA, (Withdrawn 2007)

64- ASTM D240-17 Standard Test Method for Heat of Combustion of Liquid Hydrocarbon Fuels by Bomb Calorimeter, West Conshohocken, PA, 2017, https://doi.org/10.1520/D0240-17

65- ASTM D5191-15 Standard Test Method for Vapor Pressure of Petroleum Products (Mini Method), West Conshohocken, PA, 2015, https://doi.org/10.1520/D5191-15

66- ASTM D5188-16 Standard Test Method for Vapor-Liquid Ratio Temperature Determination of Fuels (Evacuated Chamber and Piston Based Method), West Conshohocken, PA, 2016, https://doi.org/10.1520/D5188-16

67- Windom BC, Bruno TJ. Improvements in the measurement of distillation curves. 5. Reduced pressure advanced distillation curve method. Ind. Eng. Chem. Res., vol. 50, 2011, p. 1115–26. doi:10.1021/ie101784g.

68- Bruno TJ, Huber ML. Evaluation of the physicochemical authenticity of aviation kerosene surrogate mixtures. Part 2: Analysis and prediction of thermophysical properties. Energy and Fuels 2010;24:4277–84. doi:10.1021/ef1004978.

69- Smith BL, Bruno TJ. Improvements in the measurement of distillation curves. 3. Application to gasoline and gasoline + methanol mixtures. Ind Eng Chem Res 2007;46:297–309. doi:10.1021/ie060937u.

70- Burke SC., Ratcliff M, McCormick R, Rhoads R, & Windom B (2018). Measured and predicted vapor liquid equilibrium of ethanol-gasoline fuels: The influence of azeoptrope interactions on aromatic species enrichment and particulate matter formation in spark ignition engines. SAE Technical Paper Series, (2018-01-0361), In Press.

71- Ferris AM, Rothamer DA. Methodology for the experimental measurement of vapor-liquid equilibrium distillation curves using a modified ASTM D86 setup. Fuel 2016;182:467–79. doi:10.1016/j.fuel.2016.05.099.

72- ASTM D6729-14 Standard Test Method for Determination of Individual Components in Spark Ignition Engine Fuels by 100 Metre Capillary High Resolution Gas Chromatography, West Conshohocken, PA, 2014, https://doi.org/10.1520/D6729-14

73- Backhaus J, 2013, Design methodology of bio-derived gasoline fuels .M.S., Mechanical Engineering, University of Wisconsin, Madison, WI.

74- Burke SC, Ratcliff M, McCormick R, Rhoads R, Windom B. Distillation-based Droplet Modeling of Non-Ideal Oxygenated Gasoline Blends: Investigating the Role of Droplet Evaporation on PM Emissions. SAE Int J Fuels Lubr 2017;10:2017-01–0581. doi:10.4271/2017-01-0581.

75- Chupka GM, Christensen E, Fouts L, Alleman TL, Ratcliff MA, McCormick RL. Heat of Vaporization Measurements for Ethanol Blends Up To 50 Volume Percent in Several Hydrocarbon Blendstocks and Implications for Knock in SI Engines. SAE Int J Fuels Lubr 2015;8:2015-01–0763. doi:10.4271/2015-01-0763.

76- Chevron. "Motor Gasoline Technical Review", Chevron Product Company, USA, Downloaded November 2016, http://www.chevron.com/

77- Mužíková Z, Pospíšil M, Šebor G. Volatility and phase stability of petrol blends with ethanol. Fuel 2009;88:1351–6. doi:10.1016/j.fuel.2009.02.003.

78- Smith BL, Ott LS, Bruno TJ. Composition-explicit distillation curves of diesel fuel with glycol ether and glycol ester oxygenates: Fuel analysis metrology to enable decreased particulate emissions. Environ Sci Technol 2008;42:7682–9. doi:10.1021/es800067c.

79- Karonis D, Lois E, Zannikos F, Alexandridis A, Sarimveis H. A Neural Network Approach for the Correlation of Exhaust Emissions from a Diesel Engine with Diesel Fuel Properties. Energy & Fuels 2003;17:1259–65. doi:10.1021/ef020296p.

80- Rakopoulos DC, Rakopoulos CD, Giakoumis EG, Papagiannakis RG, Kyritsis DC. Influence of properties of various common bio-fuels on the combustion and emission characteristics of high-speed DI (direct injection) diesel engine: Vegetable oil, bio-diesel, ethanol, n-butanol, diethyl ether. Energy 2014;73:354–66. doi:10.1016/j.energy.2014.06.032.

81- Christensen E, Yanowitz J, Ratcliff M, McCormick RL. Renewable oxygenate blending effects on gasoline properties. Energy and Fuels 2011;25:4723–33. doi:10.1021/ef2010089.

82- Delgado RCOB, Araujo AS, Fernandes VJ. Properties of Brazilian gasoline mixed with hydrated ethanol for flex-fuel technology. Fuel Process Technol 2007;88:365–8. doi:10.1016/j.fuproc.2006.10.010.

83- Hadler AB, Ott LS, Bruno TJ. Study of azeotropic mixtures with the advanced distillation curve approach. Fluid Phase Equilib 2009;281:49–59. doi:10.1016/j.fluid.2009.04.001.

84- ASTM International. ASTM D86-17 Standard Test Method for Distillation of Petroleum Products and Liquid Fuels at Atmospheric Pressure. West Conshohocken, PA; ASTM International, 2017. doi: https://doi.org/10.1520/D0086-17

85- Aikawa K, Sakurai T, Jetter JJ. Development of a Predictive Model for Gasoline Vehicle Particulate Matter Emissions. SAE Int J Fuels Lubr 2010;3:610–22. doi:10.4271/2010-01-2115.

86- Ratcliff MA, Burton J, Sindler P, Christensen E, Fouts L, Chupka GM, et al. Knock Resistance and Fine Particle Emissions for Several Biomass-Derived Oxygenates in a Direct-Injection Spark-Ignition Engine. SAE Int J Fuels Lubr 2016;9:2016-01–0705. doi:10.4271/2016-01-0705.

87- Storch M, Koegl M, Altenhoff M, Will S, Zigan L. Investigation of soot formation of spark-ignited ethanol-blended gasoline sprays with single- and multi-component base fuels. Appl Energy 2016;181:278–87. doi:10.1016/j.apenergy.2016.08.059.

88- Design Institute for Physical Property Data (U.S.). DIPPR Project 801, full version: evaluated standard thermophysical property values. Des Inst Phys Prop Res 2005.

89- Storch M, Koegl M, Altenhoff M, Will S, Zigan L. Investigation of soot formation of spark-ignited ethanol-blended gasoline sprays with single- and multi-component base fuels. Appl Energy 2016;181:278–87. doi:10.1016/j.apenergy.2016.08.059.

90- Elkotb MM. Fuel atomization for spray modelling. Prog Energy Combust Sci 1982;8:61–91. doi:10.1016/0360-1285(82)90009-0.

91- dos Santos F, le Moyne L. Spray atomization models in engine applications, from correlations to direct numerical simulations. Oil Gas Sci Technol 2011;66:801–22. doi:10.2516/ogst/2011116.

92- Wang F, Wu J, Liu Z. Surface tensions of mixtures of diesel oil or gasoline and dimethoxymethane, dimethyl carbonate, or ethanol. Energy and Fuels 2006;20:2471–4. doi:10.1021/ef060231c.

93- Hansen AC, Zhang Q, Lyne PWL. Ethanol-diesel fuel blends - A review. Bioresour Technol 2005;96:277–85. doi:10.1016/j.biortech.2004.04.007.

94- Heuser B, Jakob M, Kremer F, Pischinger S, Kerschgens B, Pitsch H. Tailor-made fuels from biomass: Influence of molecular structures on the exhaust gas emissions of compression ignition engines. 22nd SAE Bras Int Congr Display, Bras 2013 2013;13. doi:10.4271/2013-36-0571.

95- Pumphrey JA, Brand JI, Scheller WA. Vapour pressure measurements and predictions for alcohol-gasoline blends. Fuel 2000;79:1405–11. doi:10.1016/S0016-2361(99)00284-7.

96- Elfasakhany A, Mahrous AF. Performance and emissions assessment of n-butanol–methanol–gasoline blends as a fuel in spark-ignition engines. Alexandria Eng J 2016;55:3015–24. doi:10.1016/j.aej.2016.05.016.

97- Thewes M, Müther M, Brassat A, Pischinger S, Sehr A. Analysis of the Effect of Bio-Fuels on the Combustion in a Downsized DI SI Engine. SAE Int J Fuels Lubr 2012;5:274–88. doi:10.4271/2011-01-1991.

98- Muzikova Z, Siska J, Pospisil M, Sebor G. Phase stability of butanol-gasoline blends. Chem List 2013;107:638–42.

99- Gautam M, Martin II DW, Carder D. Emissions characteristics of higher alcohol/gasoline blends. Proc Inst Mech Eng Part A J Power Energy 2000;214:165–82. doi:Doi 10.1243/0957650001538263.

100- Aikawa K (Honda RCL., Sakurai T (Honda RCL., Jetter JJ (Honda RAI. Development of a Predictive Model for Gasoline Vehicle Particulate Matter Emissions. SAE Int J Fuels Lubr 2010;3:610. doi:10.4271/2010-01-2115.